2020•2021

Faculteit Industriële Ingenieurswetenschappen

master in de industriële wetenschappen: chemie

Masterthesis

First generation of membrane distillation microchips: characterization and proof of concept

PROMOTOR :

Prof. dr. ir. Leen THOMASSEN

BEGELEIDER :

ing. Joris CLAES

Vincent Breukeleers

Scriptie ingediend tot het behalen van de graad van master in de industriële wetenschappen: chemie

Gezamenlijke opleiding UHasselt en KU Leuven

2020•2021

Faculteit Industriële Ingenieurswetenschappen

master in de industriële wetenschappen: chemie

Masterthesis

First generation of membrane distillation microchips: characterization and proof of concept

PROMOTOR :

Prof. dr. ir. Leen THOMASSEN

BEGELEIDER :

ing. Joris CLAES

Vincent Breukeleers

Scriptie ingediend tot het behalen van de graad van master in de industriële wetenschappen: chemie

UHASSELT

KU LEUVEN

Acknowledgements

First and foremost, I want to express my sincerest gratitude to the promoter of this research, prof. dr. ir. Leen Thomassen, who provided me with the opportunity of deepening my knowledge regarding membrane distillation processes. I also want to thank her for all the support she gave me throughout this thesis, as her great advice, amazing feedback and words of encouragement in time of need were always just what I needed.

Additionally, I want to thank prof. dr. ir. Wim De Malsche and ir. Jo Wim Christiaens for their constructive feedback on the writing and their guidance during the experiments. Their insight often opened new perspectives on how I looked at my results, for which I am beyond grateful. I must also express gratitude to the µFlow group (VUB, lead by prof. dr. ir. Wim De Malsche) for letting us use their membrane microcontactor during the experimental phase, without which this research would not have been possible.

Last but not least, I want to express my sincerest gratitude to my supervisor, ing. Joris Claes, who was always there for me during the experimental phase. Whenever I encountered problems, he was there to help and advise me. Therefore, I am eternally grateful to have him with me during the entire project, not only for his knowledge and great advice but also for keeping this stressful period fun and enjoyable.

Table of contents

List of tables

List of figures

Nomenclature

Abbreviations		
Symbol	Definition	Unit
AGMD	Air Gap Membrane Distillation	-
CIPT	Centre for Industrial Process Technology	-
DCMD	Direct Contact Membrane Distillation	-
GC	Gas Chromatography	-
GC-FID	Gas Chromatography Flame Ionization Detector	-
ID	Inner Diameter	-
LEP	Liquid Entry Pressure	-
MD	Membrane Distillation	-
MF	Micro Filtration	-
MMC	Membrane Microcontactor	-
OD	Outer Diameter	-
PFA	Perfluoro alkoxy alkanes	-
PP	polypropylene	-
PTFE	polytetrafluoroethylene	-
PVC	Polyvinyl chloride	-
PVDF	polyvinylidene fluoride	-
RO	Reversed Osmosis	-
SGMD	Sweeping Gas Membrane Distillation	-
TP	Temperature Polarization	-
TSGMD	Thermostatic Sweeping Gas Membrane Distillation	-
UF	Ultra Filtration	-
VHG	Very High Gravity	-
VMD	Vacuum Membrane Distillation	-
VOC	Volatile Organic Component	-

Symbols		
Symbol	Definition	Unit
d_h	Hydraulic diameter feed inlet channel	m
H	Total heat transport coefficient	J/s
h_m	Membrane heat transport coefficients	J/s
h_p	Permeate heat transport coefficients	J/s
h_r	Retentate heat transport coefficients	J/s
J	Transmembrane flux	ml/min
K	Total mass transport coefficient	g/s
k_g	Gas thermal conductivity	W/mK
k_l	Thermal conductivity of the feed	W/mK
k_m	Membrane mass transport coefficients	g/s
k_m	Membrane thermal conductivity	W/mK
k_r	Retentate mass transport coefficients	g/s
k_s	Polymer thermal conductivity	J/m
Nu	Nusselt number	-
P_p	Permeate Pressure	bar
P_r	Prandtl number	-

P_r	Retentate pressure	bar
Q_m	Total heat transport through the membrane	J
Q_r	Conductive heat transport retentate side	J
R	Fiber radius	m
r	Ratio of rough over smooth surface area	-
Re	Reynolds number	-
r_{max}	Maximal pore radius	m
r_{min}	Smallest pore radius	m
T_{br}	Bulk temperature retentate side	°C
T_{ip}	Membrane interface temperature permeate side	°C
T_{ir}	Membrane interface temperature retentate side	°C
α	Correction angle	°
β	Pore geometry coefficient	-
γ_L	Liquid surface tension	mN/m
γ_{LG}	Liquid-Gas interfacial tension	mN/m
γ_{SG}	Solid-Gas interfacial tension	mN/m
γ_{SL}	Solid-Liquid interfacial tension	mN/m
δ	Membrane thickness	m
ΔH_v	Evaporation heat	J
$\Delta P_{interface}$	Interfacial pressure difference	bar
ΔT_m	Temperature difference over the membrane	°C
ε	Porosity	-
θ	Contact angle	°
θ'	effective contact angle	°
ρ_m	Membrane density	kg/m^3
ρ_{pol}	Polymer density	kg/m^3
τ	Tortuosity	-

Abstract

Although membrane distillation (MD) has several advantages over conventional recovery techniques, it is used in the industry to a limited extent due to a couple of drawbacks such as fouling, uncertainties regarding operational costs and breakthrough. The latter, which is the phenomenon where the membrane gets wetted by the solvent, undermines the working principle of MD as the feed solvent no longer gets retained at the retentate side of the membrane. As to prevent this from happening, the transmembrane pressure must be kept below a critical threshold, generally called the liquid entry pressure (LEP). So far, a couple of empirical equations have been proposed which obtained an average deviation of 25.0% at best. Within this research, the most recent LEP correlation by Hereijgers et al. (2015) was evaluated for aqueous solutions, containing organic components (i.e. methanol, ethanol, acetone, acetic acid and acetonitrile), using a membrane microcontactor. Four different parameters were evaluated, resulting in a positive relation with the LEP for both the contact angle (θ) and the surface tension (γ_L), while the concentration and the Kamlet-Taft polarity factors showed a negative relation with the LEP. All of this resulted in a proposed correlation to predict the maximum allowable pressure with an average deviation of 24,53%: $LEP=-0.0459\ \gamma_L \cos(\theta+0.937)$.

Additionally, a vacuum membrane distillation (VMD) experiment was performed and possible improvements to enhance the performance of the setup were discussed.

Abstract in Dutch

Desondanks dat membraan destillaties (MD) verschillende voordelen heeft ten opzichte van conventionele zuiveringstechnieken, wordt het slechts in beperkte maten gebruikt in de industrie ten gevolgen van enkele nadelen zoals vervuilingen, onzekerheden omtrent productie kosten en doorslag. Dit laatste nadeel, ook gekend als het fenomeen waarbij het membraan bevochtigd wordt, ondermijnt het werkingsprincipe van MD doordat de voedingsstroom niet langer tegengehouden aan de retentaat zijde van het membraan. Om dit te voorkomen moet het drukverschil over het membraan onder een kritische grens gehouden worden, die ook wel de liquid entry pressure (LEP) genoemd wordt. Tot dusver zijn er reeds een aantal empirische vergelijkingen voorgesteld die, in het beste geval, een gemiddelde afwijking van 25.0% gaven. In dit onderzoek wordt de meest recente vergelijking, Hereijgers et al. (2015), geëvalueerd voor waterige mengsels die steeds een organische component bevatten (zoals methanol, ethanol, azijnzuur, aceton en acetonitril) met behulp van een membraan microcontactor. Hierbij werden vier verschillende parameters geëvalueerd, wat tot resultaat had dat de LEP een evenredig verband toonde met de contacthoek (θ) en de oppervlakte spanning (γ_L), terwijl een omgekeerd evenredig verband aangetoond kon worden met zowel de concentratie van de organische component als met de Kamlet-Taft polariteitsfactor. Dit alles resulteerde in een voorgestelde vergelijking voor het voorspellen van de LEP, dewelke een gemiddelde afwijking vertoonde van 24.53%: $LEP=-0.0459\ \gamma_L \cos(\theta+0.937)$.

Aanvullend werd er nog een vacuüm membraan destillatie uitgevoerd en werd deze opstelling geëvalueerd en besproken voor mogelijke prestatieverbeteringen.

1. Introduction

1.1. Context

Membrane distillation (MD) is a thermally driven process that uses (micro)porous hydrophobic or hydrophilic membranes as a barrier to retain the less-volatile components at the retentate side. By applying a thermal gradient across the membrane, a difference in vapour pressure is created between both membrane surfaces which serves as the driving force for all transport through the membrane. Due to the nature of the membranes, only vapours are allowed to diffuse through the membrane pores as liquids are retained at the retentate side because of surface tension forces. This results in vapour-liquid interfaces being formed at the pore entrances [1]–[3].

When comparing MD to other separation processes, it has a couple of advantages over its competitors. One is that it the possible to (theoretically) remove 100% of all non-volatile components (e.g. ions, colloids) and the other is that its operating temperature and pressure will be lower in comparison to distillation and pressure-driven membrane separation processes respectively [1], [4]. Also, lower operating temperatures provide the possibility to use waste heat and/or alternative energy sources such as solar energy, geothermal energy and waste grade energy from low temperature industrial streams which could drastically decrease the overall energy consumption [2].

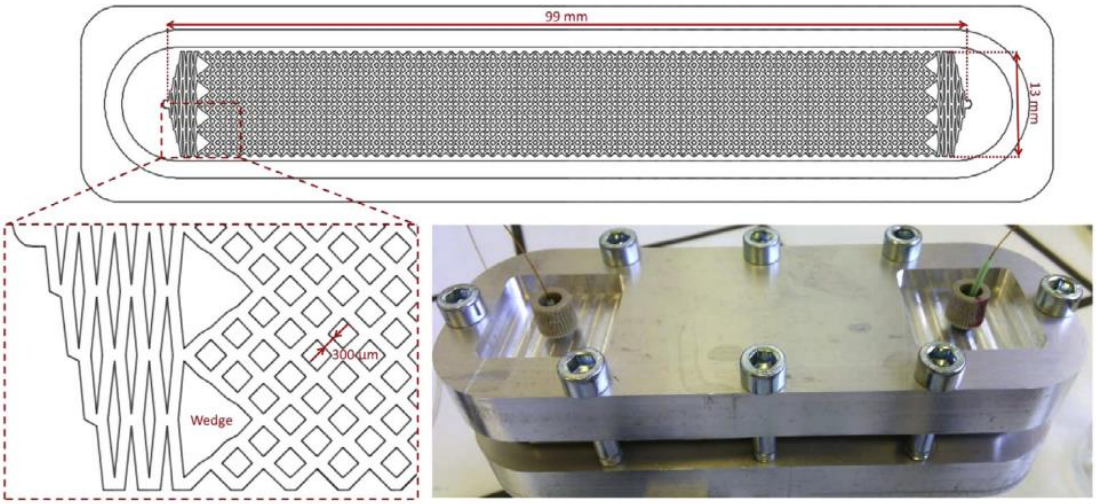

Figure 1: Schematic view of MMC, both on the inside and the outside [5]

Although the concept of MD was first patented in 1963 by Bruce R. Bodell [6], its implementation in the industry is limited. In collaboration with the µFlow group of the VUB who provided a membrane microcontactor (MMC, Figure 1) for this research, the CIPT research group (KU Leuven) aims to establish MD as a viable alternative for the more conventional separation techniques by utilising it either as an *ex-situ* or an *in-situ* recovery method. So far, the *in-situ* application of MD has been explored to a limited extent. Non the less, some researchers provided promising results for this topic. In 2017, Zhang et al. [7] used a combination of very high gravity (VHG) technology with *in-situ* vacuum membrane distillation (VMD) to instantaneously remove ethanol, produced by

immobilized *Zymomonas mobilis* cells. Their results outperformed all other methods found in the literature.

1.2. Problem definition

As was mentioned before, the concept of MD is used to a limited extent within the industry. This can be related to several different reasons such as a relatively low permeate flux in comparison to other separation techniques; a decrease in permeate flux due to concentration and temperature polarization effects, membrane fouling and total or partial pore wetting; the used membrane; module design and high energy consumption which causes uncertainty regarding energy and economical costs [1].

Since tackling all these issues at once would be an immense work, this thesis will only focus on the breakthrough principle within the provided MMC. The phenomenon of breakthrough can be defined as when the feed solvent is no longer retained at the pore openings due to the pressure exceeding a critical threshold. Instead of only vapour, liquid also will be moved to the other side of the membrane which undermines the entire separation process and must be avoided at all cost.

To define this threshold, a lot of different empirical models were proposed throughout the years. The overall most used model throughout the literature to predict this so-called liquid entry pressure (LEP) is the Young-Laplace law (Eq. 1) [8], [9]:

$$LEP = -\frac{2\beta\gamma_L \cos\theta}{r_{max}} \tag{1}$$

Where β represents the pore geometry coefficient, γ_L represents the liquid surface tension [Nm-1], θ is the contact angle [°] and r_{max} represents the maximal pore radius [m]. This model, along with the Kim et al. model [10], [11] which proposed an equation for non-cylindrical pores and the Zha et al. model [11], [12] which assumed the pore geometry to be axially irregular, has been evaluated by Hereijgers et al. in 2015. Within their research, a new correlation was developed (based on the original Young-Laplace law) to calculate the LEP value using two fitting parameters α and β which are correction factors for the contact angle and the pore geometry respectively [13]:

$$LEP = -\frac{2\gamma_L\beta \cos(\theta + \alpha)}{r_{max}} \tag{2}$$

Although this model reduces the deviation to 25.0%, which is considerably lower than the original Young-Laplace law that had a deviation of 37.5%, it is far from perfect. Therefore, the Hereijgers model will be evaluated and optimized to develop a more accurate equation for the calculation of the LEP.

1.3. Research objectives

The main objective of this research is to propose an empirical model for the determination of the LEP threshold, which should improve the accuracy for LEP predictions in comparison to the model of Hereijgers et al. [13]. The eventual model will most likely be

another adaptation of the Young-Laplace law (Eq. 1) in which the current Hereijgers equation (Eq. 2) will be further expanded.

First and foremost, the correlation between the LEP-values and the parameters from the Hereijgers equation (contact angle and surface tension) must be evaluated to define their impact and confirm that their finding can be reproduced. Once this has been done, other parameters can be analysed to assess their influence. This will be done in the form of a thorough literature study which should provide as much information about both mixture and membrane properties (e.g., density, polarity) and mixture-membrane interactions as possible to assess whether these have a direct impact. In case a certain parameter does directly affect the LEP, the individual parameters could be taken into the equation to decrease the impact from correction factors such as α and β which diminish the accuracy.

Within this literature study, it is important to evaluate the parameters and interactions which will not be addressed during the experimental phase. Except for the properties of both pure solvents and the used mixtures, it is important to evaluate other things such as the impact of the type of used membranes and the effect it has on the pore size factor.

Once all experimental data is combined with the additional mixture properties, a model will be proposed, based on the four proposed solvent mixtures (i.e. methanol-water, ethanol-water, acetic acid-water and acetone-water), which will be evaluated by a proof of concept. Here, a fifth solvent system (acetonitrile-water) will be used to validate the proposed model along with additional data found in the literature.

2. Literature study

Within this section, a brief background for membrane distillation processes is provided. It starts with an explanation of the general concept of MD, followed by the possible MD configurations and their applications. From there on, the focus lies primarily on vacuum membrane distillation, providing a brief section about its heat and mass transport phenomena. Afterwards, both the important operating parameters and membrane properties are discussed to address possible improvements for further MD processes. Eventually, the focus shifts toward pore wetting where both the phenomenon is described as well as important parameters and previous work.

2.1. General concept of membrane distillation

Membrane distillation (MD) is often described as an emerging non-isothermal membrane separation process, mainly used for aqueous solutions, in which at least one side of the membrane is in direct contact with the feed solution. As is shown in Figure 2, vapour is transferred through the membrane pores to the permeate side while the feed solution is restrained at the pore entrances at the retentate side because of surface tension forces. These surface tension forces, caused by the hydrophobic nature of the membrane, create a vapour-liquid interface where the more volatile components are allowed to evaporate and move through to the permeate side. This entire process is driven by a difference in vapour pressure, which in turn is caused by a thermal gradient over the (micro)porous hydrophobic membrane [1]–[3].

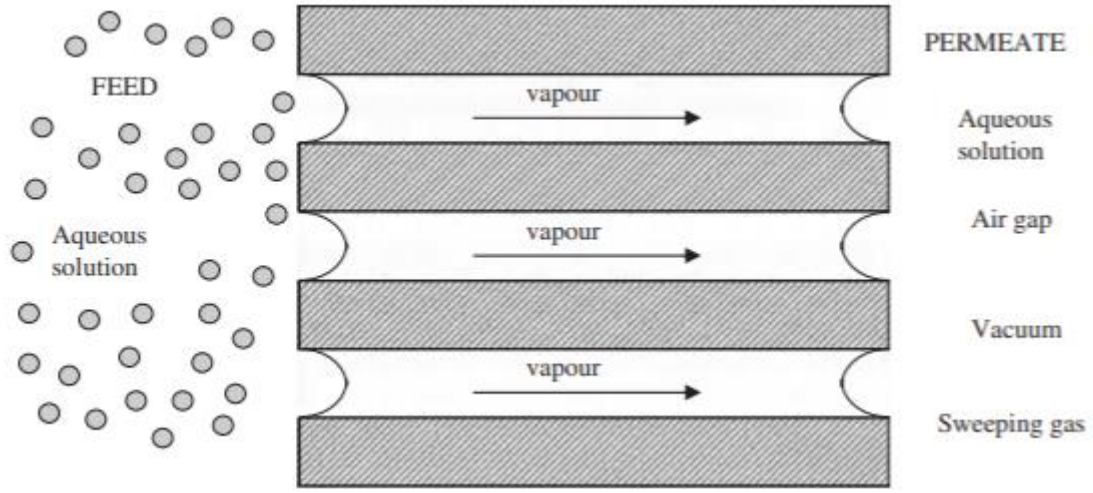

Figure 2: Schematic representation of MD concept [14]

Although the industrial implementation of MD is limited, it offers several different advantages over conventional separation techniques. First and foremost, MD can be utilised as a compact recovery process as, in contrast to conventional distillation which required high vapour velocities to ensure enough vapour-liquid contact and therefore needs larger installations, MD uses a microporous hydrophobic membrane to support a vapour-liquid interface [4], [15]. Second, the operating temperatures for MD are almost always much lower than conventional separation techniques, since it is unnecessary to

heat the feed solution to its boiling point. In general, MD is often operated at a temperature between 30 and 90°C which (in combination with the compact processing unit) decreases the amount of heat loss to the environment. Additionally, since the operating temperatures are much lower, waste heat and/or alternative energy sources such as solar energy, geothermal energy and waste grade energy from low temperature industrial streams can be used as an alternative heating source [2], [4]. Finally, MD also has an advantage over conventional pressure-driven processes such as reversed osmosis (RO), microfiltration (MF) and ultrafiltration (UF) since it is a thermally driven process. This allows MD to be operated at much lower pressures, generally on the order of zero to a hundred kPa, which leads to an overall lower equipment cost and increases the general safety of the process. Also, since MD relies on the principle of vapour-liquid equilibrium, 100% (theoretical) of ions, macromolecules, colloids, cells, and other non-volatile components can be rejected which has so far been impossible to achieve with either RO, MF or UF [4].

Overall, MD offers plenty of advantages over the conventional separation techniques which has made it an interesting process, mainly from an academic perspective. Although several different applications (i.e. desalination of seawater, treatment of wastewater, concentration of fruit juices, etc.) have been intensely studied at the development stage of laboratory, the attempts to implement it on a commercial scale are rather scarce due to difficulties in engineering aspects and relatively large operating costs [16], [17].

2.2. Different configurations

Although the retentate (feed) side of MD always stays the same, there are several different options for the permeate side which leads to some different configurations. The most commonly known are direct contact membrane distillation (DCMD), air gap membrane distillation (AGMD), sweeping gas membrane distillation (SGMD) and vacuum membrane distillation (VMD) of which the advantages and disadvantages are summarised in Table 1. There are also several different hybrid configurations, which will not be included in this literature study.

Table 1: Advantages, disadvantages and application areas of different MD configurations [18]

Configuration type	Advantages	Disadvantages
DCMD	High permeate flux Considered at commercial scale	Heat loss by conduction
AGMD	Low conductive heat loss Simple process Little chance of developing temperature polarization (TP)	Lower permeate flux when compared to DCMD and VMD
SGMD	Less resistance to mass transfer through forced flow	Possibility of developing temperature polarization (TP) Complex process
VMD	High permeate flux Considered at commercial scale	Increased risk of wetting membrane pores Complex process

2.2.1. Direct contact membrane distillation

Direct contact membrane distillation (DCMD), as is shown in Figure 3, uses both a hot (feed) solution at the retentate side and a cold solution at the permeate side. By having the feed solution in direct contact with the hot membrane surface side, volatile components are allowed to evaporate. The then formed vapour will, under the influence of a pressure difference over the membrane, be transported to the permeate side where it condenses. Due to the nature of the membrane, the feed solution will not be allowed to penetrate the membrane pores [19], [20].

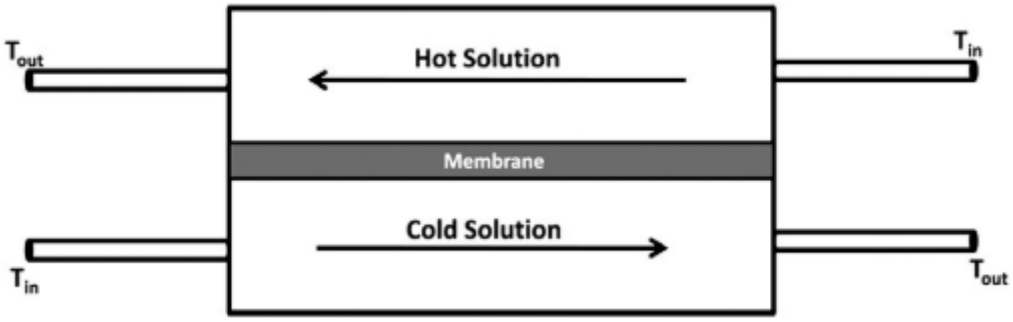

Figure 3: Direct contact membrane distillation (DCMD) [19]

DCMD is generally described as the most simple MD configuration, as it is capable of carrying out the condensation step within the MD module and provides high permeate fluxes. The downside of this configuration is that heat will be transferred through the membrane, which is considered heat loss. Its applications range from desalination of seawater and concentration of aqueous solutions for food applications to acid manufacturing [19].

2.2.2. Air gap membrane distillation

Figure 4 shows a schematic diagram of air gap membrane distillation (AGMD). This type of configuration utilizes a stagnant air gap between the membrane surface at the permeate side and the cold condensation surface. This air gap, which has a temperature higher than the hot (feed) solution and lower than the condensation surface, will keep the total heat transfer through the membrane at a minimum. Unfortunately, it also serves as additional resistance to the mass transfer, decreasing the total flux to the permeate side [19], [21].

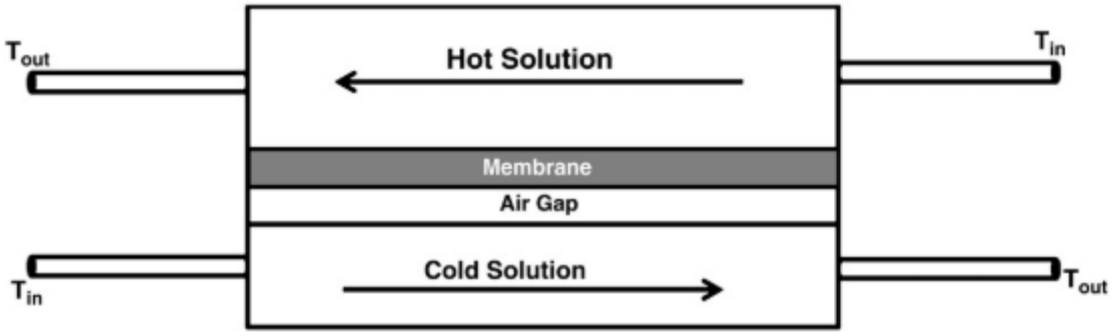

Figure 4: Air gap membrane distillation (AGMD) [19]

The general applications for AGMD are desalination and removing volatile components from aqueous solutions. Additionally, AGMD has also been described as a method to break azeotropic mixtures [21].

2.2.3. Sweeping gas membrane distillation

Figure 5 displays sweeping gas membrane distillation (SGMD) which utilizes an inert gas to drag all vapour, coming through the pores, out of the MD unit to an external condenser. Just as with AGMD, the gas barrier decreases the total heat loss through the membrane but since the gas layer is not stationary, the additional resistance to the mass transport can be avoided. This type of configuration is therefore mainly used for removing volatile components from aqueous solutions [19].

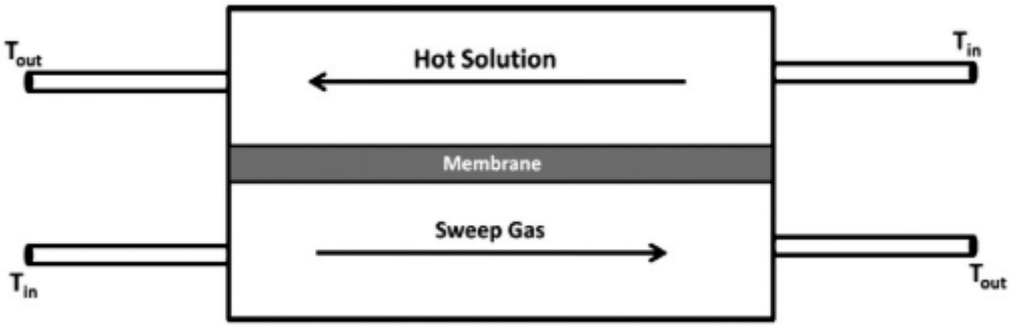

Figure 5: Sweeping gas membrane distillation (SGMD) [19]

Unfortunately, since the sweeping gas temperature increases between the inlet and outlet, the mass transfer and heat transfer rate through the membrane change dramatically during the gas circulation along the membrane module [22]. Therefore, a combination of SGMD and AGMD was proposed to decrease temperature fluctuations of the carrier gas. This so-called thermostatic sweeping gas membrane distillation (TSGMD, Figure 6) uses both a cooled condensation surface and a sweeping gas which allows the vapour to condense either in the MD unit or in the external condenser [15], [18], [19], [22].

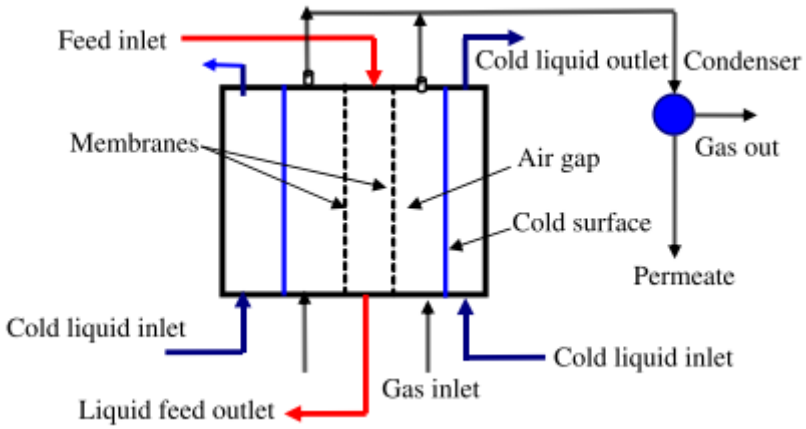

Figure 6: Thermostatic sweeping gas membrane distillation (TSGMD) [22]

2.2.4. Vacuum membrane distillation

Vacuum membrane distillation (VMD, Figure 7) uses a pump to apply a low pressure or vacuum at the permeate side of the MD module. All vapour that comes through the pores is dragged along to an external condenser which increases the complexity of the process. in general, VMD is regarded as one of the more interesting configurations due to a high energy efficiency (as there is no medium at the permeate side for heat to diffuse through) and larger fluxes (due to an increase in transmembrane pressure difference) in comparison to the other configurations [23]. Overall, the removal of volatile components from aqueous solutions is the most noticeable application of VMD [3], [19].

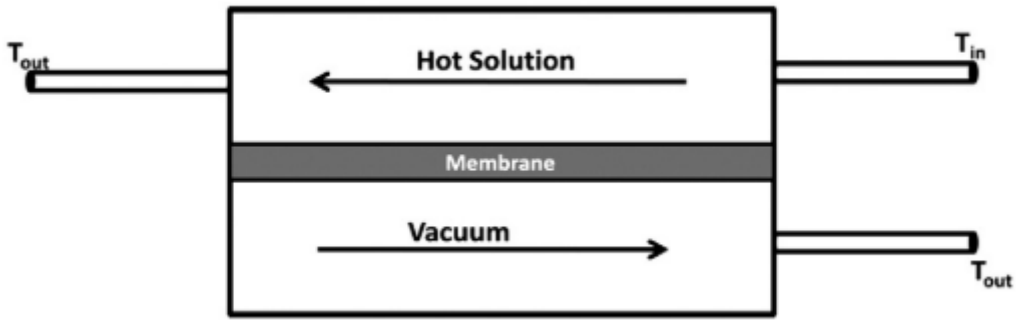

Figure 7: Vacuum membrane distillation (VMD) [19]

2.2.4.1. Heat transport in VMD

The heat transport of MD is generally divided into three different consecutive steps which are (1) conductive heat transport from the feed bulk towards the boundary layer at the membrane surface, (2) heat transfer either by conduction through the membrane itself or by transport alongside the vapour which moves through the membrane pores (i.e. latent heat of evaporation) and (3) convective heat transport at the permeate side. All this can be regarded as a series of resistances, which is depicted in Figure 8 and describes in equation 3a [24]:

$$\frac{1}{H} = \frac{1}{h_r} + \frac{1}{h_m + J\Delta H_v/\Delta T_m} + \frac{1}{h_p} \qquad (3a)$$

which correlates the total heat transport coefficient (H) to h_r, h_m, h_p (the heat transport coefficients of the retentate, membrane and permeate respectively), J (transmembrane flux), ΔH_v (evaporation heat) and ΔT_m (temperature difference over the membrane). It is important to mention that, when regarding VMD, the resistance at the permeate side is neglectable as there is no convection at the permeate side due to the absence of any type of fluid. Equation 3a can therefore be adjusted for VMD purposes, which leads to equation 3b [24]:

$$\frac{1}{H} = \frac{1}{h_r} + \frac{1}{h_m + J\Delta H_v/\Delta T_m} \qquad (3b)$$

To calculate the effective heat transport within the VMD module, both the conductive heat transport from the feed bulk towards the boundary layer at the membrane surface and

the heat transfer either by conduction through the membrane itself or by transport alongside the vapour which moves through the membrane pores must be addressed. When regarding the conductive heat transport at the retentate side, it is generally calculated as described in equation 4 [1], [25], [26]:

$$Q_r = h_r(T_{b,r} - T_{I,r}) \tag{4}$$

where $T_{b,r}$ and $T_{I,r}$ represent the temperature of the bulk and membrane surface at the retentate side, respectively. To retrieve the retentate heat transport coefficient (h_r), most publications rely on existing empirical correlations for an estimation, of which the Nusselt number (Nu) is the most frequently used (Eq. 5) [24]:

$$Nu = \frac{h_r d_h}{k_L} = aRe^b Pr^c \tag{5}$$

where d_h is the hydraulic diameter of the feed inlet channel; k_L represents the thermal conductivity of the feed; a, b and c are constants that correspond to the MD design and the flow regime; Re and Pr are the Reynolds and Prandtl number respectively.

Besides the heat transfer from the bulk to the boundary layer, there is also heat moving from one side of the membrane to the other. As mentioned before, this heat transport can either happen by conduction through the membrane or by transport alongside the vapour. Therefore, both possibilities are taken into consideration when calculating the heat transport (as can be seen in equation 6a) [24]:

$$Q_m = J\Delta H_v + \frac{k_m}{\delta}(T_{I,r} - T_{I,p}) \tag{6}$$

where k_m and δ are membrane properties (i.e. thermal conductivity and thickness respectively, which will be discussed later), while $T_{I,r}$ and $T_{I,p}$ are the temperatures at the membrane surface at the retentate and permeate side, respectively.

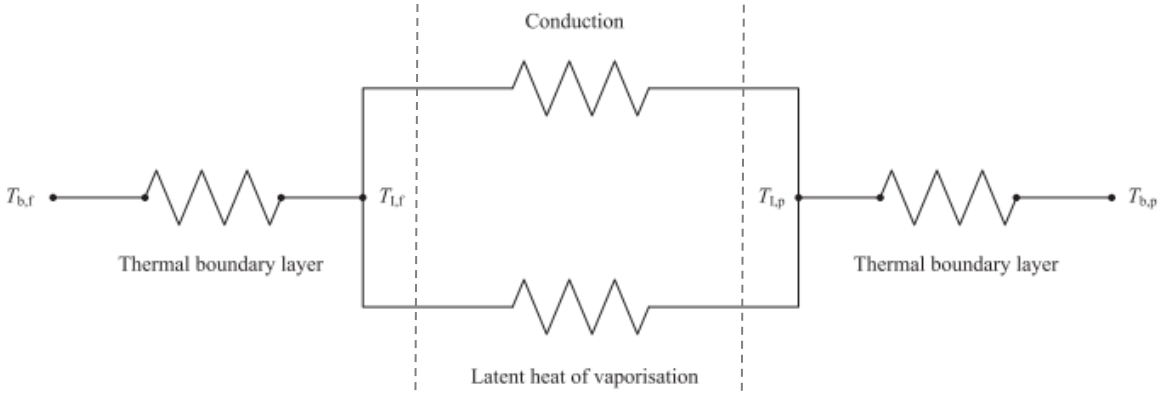

Figure 8: Schematic representation of heat transport resistances for MD with the retentate side (left), membrane (middle) and permeate (right) [24]

2.2.4.2. Mass transport in VMD

Similar to heat transport, mass transport consists of three consecutive steps: (1) diffusion from the retentate bulk to the membrane surface, (2) evaporation of the volatile

component at the liquid-vapour interface that then moves through the membrane pores and (3) diffusion from the permeate membrane surface into the permeate stream as depicted in Figure 9. Once again, just as with the heat transport, the presence of the vacuum decreases the overall resistance to mass transfer at the permeate side. therefore, it is generally accepted that the total resistance to mass transport can be described as follows (Eq.7) [27], [28]:

$$\frac{1}{K} = \frac{1}{k_r} + \frac{1}{k_m} \tag{7}$$

which correlates the total mass transport coefficient (K) to $k_r$and k_m (i.e. mass transport coefficients of the retentate and membrane, respectively).

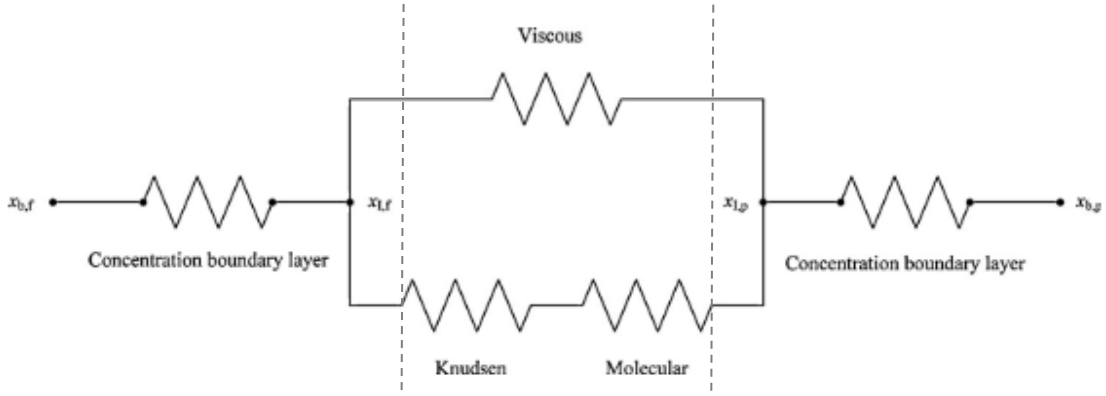

Figure 9: Schematic representation of mass transport resistances for MD retentate side (left), membrane (middle) and permeate (right) [24]

2.3. Impact of operating parameters

When operating MD processes, several different parameters will have a significant influence on the performance of MD. The most important parameters for MD are discussed in this section to provide some insight on how to optimise beneficial parameters such as flux while keeping malefactors (e.g. temperature and concentration polarisation) at a minimum. Below, a summary of the effects of most operating parameters on the transmembrane flux (for the general four types of MD) is given in Table 2.

Table 2: Summary of effects of different operating parameters on flux for conventional MD configurations [1]

Parameter	DCMD	AGMD	SGMD	VMD
Feed temperature	↗	↗	↗	↗
Feed concentration (non-volatile)	↘	↘ or ↔	↘	↘
Feed concentration (volatile)	↗	↗	↗	↗
Feed flow rate	↗ or ↷	↷	↗ or ↔	↗ or ↷
Feed mixing	↗	⊗	⊗	↗
permeate temperature	↘	↔ or ↘	↘ or ↔	⊗
permeate flow rate	↗ or ↔	↔	↷	⊗
vapour pressure difference	↗	↗	↗	↗

↗: increases with, ↘; decreases with, ↔: insignificant impact, ↷: reaches optimal value or asymptotic level, ⊗: impact irrelevant or unknown

2.3.1. Feed temperature

Independent of which type of configuration is used for the MD process, increasing the temperature of the feed solution will cause an exponential increase in vapour pressure at the retentate side of the membrane. As the vapour pressure increases at the retentate side, the difference in vapour pressure over the membrane (i.e. the driving force) will also increase exponentially with an increase in temperature. Since the flux over the membrane is directly correlated to the driving force, the flux increases exponentially when increasing the temperature [1], [18], [29].

Besides the effect on the flux, an increase in temperature will also make way for temperature polarization effects to take place as the temperature difference over the membrane is enlarged. This drastically decreases the efficiency of MD as it leads to more heat loss (i.e. heat transfer through the membrane instead of being used for evaporation) which must be kept at a minimum [1].

2.3.2. Feed concentration

When regarding the influence of the feed concentration on the MD process, a clear difference is made between aqueous solutions containing non-volatile components and those containing volatile components. For the volatile component solutions, an increase in concentration seems to decrease the flux (for any type of MD configuration) as this causes the vapour pressure to decrease. Also, the addition of more non-volatile components can cause concentration polarisation (i.e. accumulation of non-volatile components at the membrane surface) but this effect is rather small in comparison to the effect of temperature polarization [1], [30], [31]. For the volatile component solutions (e.g. alcohols), the effect of increasing the concentration is rather dependent on its interaction with water and the thermodynamic properties of the volatile component. In most cases, increasing the concentration of the volatile component leads to a higher flux as the transmembrane partial pressure of the volatile component is increased. This often goes alongside two different issues. First, the increase of volatile components often increases the risk of pore wetting as the membrane is mostly resistant to water only. Second, the presence of non-volatile components in binary aqueous mixtures can change the vapour pressure of the mixture resulting in a change in selectivity [1], [32].

2.3.3. Feed flow rate and mixing

Regarding the flow rate and the mixing of the feed within the reactor, a clear difference must be made between DCMD, AGMD and VMD on one side and SGMD on the other. For DCMD, AGMD and VMD, increasing the flow rate and mixing will cause the permeate flux to increase, which in some cases has proven to reach an asymptotic maximum [32]–[34]. This is because increasing the flow rate and mixing at the retentate side leads to less temperature and concentration polarisation while simultaneously increasing the heat transfer coefficient. It is therefore generally accepted that a turbulent flow is advised for these configurations as it ensures a smaller temperature difference between the bulk and

the membrane surface, which provides a higher temperature difference over the membrane [31], [35]–[38]. For SGMD however, this is not the case as the effects of concentration polarization (when using non-volatile components) at the retentate side is insignificant in comparison to that at the permeate side so changing either the mixing or flow rate of the feed will have a negligible effect on the transmembrane mass transport [39], [40].

It is worth mentioning that the presence of volatile components in the feed mixture will ensure that the separation factor enhances as the flow rate increases. This is because better mixing will subdue the concentration polarisation at the membrane surface [34], [41].

2.3.4. Vapour pressure difference

To create a transmembrane vapour pressure difference, either a temperature difference over the membrane, a vacuum or a combination of both can be utilised. For all types of MD, the permeate flux has shown to be linearly related to the vapour pressure difference over the membrane and has a non-linear correlation in regards to the bulk pressure difference. When focussing on VMD, increasing the transmembrane pressure difference by lowering the vacuum pressure will increase the permeate flux at the cost of the separation efficiency when regarding aqueous mixtures containing volatile organic components (VOC). Also, it must be taken into account to not exceed the liquid entry pressure as this would lead to pore wetting and would decrease the separation efficiency even more. It is therefore recommended to ensure that the vacuum pressure is larger than the vapour pressure of the volatile component [1], [42].

2.4. Membrane properties

Several hydrophobic porous membranes used for MD purposes are commercially available membranes made out of polymer materials such as polypropylene (PP), polyvinylidene fluoride (PVDF) and polytetrafluoroethylene (PTFE). To ensure good working MD processes, the membranes should have a low resistance to mass transfer, a high resistance to pore wetting, low thermal conductivity to minimise heat loss, good thermal stability and chemical resistance in regards to the used solvents [1]. All discussed membrane properties are summarised in Table 3.

Table 3: Summary of effects of different membrane properties on flux for conventional MD configurations [1]

Parameter	DCMD	AGMD	SGMD	VMD
Membrane thickness	↘ or ↷	↔	↘	↘
Porosity	↗	↗	↗	↗
Tortuosity	↘	⊗	⊗	↘
Pore size	↗	↗	↗	↗
Pore size distribution	⊗	⊗	⊗	↘
thermal conductivity	↘	↘	↘	↘

↗: increases with, ↘; decreases with, ↔: insignificant impact, ↷: reaches optimal value or asymptotic level, ⊗: impact irrelevant or unknown

2.4.1. Membrane thickness

To ensure a sufficient flux through the membrane, the thickness of those membranes should be minimized as there is an inversely proportional correlation between both. By doing so, the mass transfer resistance of the membrane would be decreased, leading to higher permeate fluxes, but it would also decrease the total resistance to the heat transfer which will cause heat losses to increase[1], [19]. According to Lagana et al., the optimal membrane thickness should be within the range of 30 to 60 μm [43].

2.4.2. Membrane porosity

The porosity of a membrane, often referred to as the void volume fraction which generally lies between 30 and 80% [1], is directly correlated to the MD flux as it impacts the surface area where the volatile components can evaporate. Additionally, filling the pores with gasses that have lower heat conduction coefficients than the membrane, will also decrease the heat transfer through the membrane which reduces heat losses [4], [44]. Smolders and Franken [45] have given an equation to calculate the porosity (ε):

$$\varepsilon = 1 - \frac{\rho_m}{\rho_{pol}} \tag{8}$$

which utilises both the membrane density (ρ_m) and the polymer density (ρ_{pol}).

2.4.3. Membrane tortuosity

The membrane tortuosity (τ), which is used to reflect how much the pore shape differs from a perfectly cylindrical shape, is generally estimated using empirical correlations such as equation (9) [25]:

$$\tau = \frac{(2 - \varepsilon)}{\varepsilon} \tag{9}$$

In general, higher tortuosity values lead to a lower flux as the vapours need to diffuse through a more difficult path which increases the overall mass transfer resistance [1], [46], [47].

2.4.4. Pore size and pore size distribution

Generally, MD processes will utilize membranes with pore sizes ranging from 50 nm up to 1 μm [48]. It must be mentioned that, for polymer membranes, the actual pore size will vary from pore to pore. Therefore, it is often advised to use either mean pore sizes or even a pore size distribution when calculating the actual transmembrane flux and vapour transfer. Overall it is accepted that using a large pore size will increase the mass transfer and flux through the membrane due to an increase in evaporation surface. However, it does also increase the chance of pore wetting which must be avoided at all cost. Therefore, the pore sizes should be evaluated for every mixture individually to find their given optimum [19].

2.4.5. Thermal conductivity

As mentioned above, increasing the thickness and the porosity of the membrane should decrease the heat losses due to additional resistance to heat transfer. Unfortunately, increasing thickness will negatively influence the permeate flux while increasing the porosity enhances the probability of creating pore wetting although this would increase mass transfer. Alternatively, heat loss can be minimized by using modified membranes which either use hydrophobic materials with lower thermal conductivities or multi-layered materials [49], [50]. The latter can contain a small hydrophobic layer on top of stronger carrier materials which adds an extra layer, thereby increasing the total resistance to heat transfer [49].

To calculate the effective thermal conductivity of a membrane, both the thermal conductivity of the polymer material (k_s) and that of the gas (k_g) are taken into account. For polymers such as PTFE, PP and PVDF, k_s is defined by the temperature, the crystal shape and crystallinity degree of the material [19]. The actual calculation can be done, using two different equations either based on volume averages of both conductivities (Eq. 10a) or based on the volume averages of both resistances (Eq. 10b) [51]:

$$k_m = (1 - x)k_s + xk_g \tag{10a}$$

$$k_m = \left[\frac{x}{k_g} + \frac{(1 - x)}{k_s}\right]^{-1} \tag{10b}$$

2.5. Pore wetting

Pore wetting refers to the phenomenon where the feed mixture is allowed to penetrate within the membrane pores which undermines the separation process of MD. This can be due to partial or complete wetting, which decreases the permeate flux due to the formation of a boundary layer that (partially) removes the hydrophobicity of the membrane or increasing the flux by creating a solvent bridge between both membrane surfaces respectively. While partial wetting occurs due to organic and/or inorganic fouling within the pore, complete wetting is caused by applying a transmembrane pressure difference that exceeds the LEP critical threshold. Other causes are also probable (but less prominent) and are given in Table 4 alongside the two previously mentioned causes.

Table 4: Possible causes of pore wetting in MD [52]

Cause	Operational condition
Transmembrane pressure	Higher than LEP
Capillary condensation	Loss of temperature gradient
Scale deposition (inorganic fouling)	Reducing the hydrophobicity of membrane
Organic fouling	Reducing the hydrophobicity of membrane
	Lowering the surface tension
Surfactants	Decreasing surface tension
Membrane degradation during long-term operation	Formation of hydrophilic groups on the membrane surface

2.5.1. Wetting mechanism

Membrane wetting can occur when the pressure balance within the membrane pores, which causes the formation of a liquid-vapour interphase, is disturbed by one of the possible causes given in Table 4. This allows the liquid solutions to enter the pores and form a water bridge through the membrane. The wetting of membranes is generally divided into four different stages: non-wetted, surface-wetted, partially-wetted, and fully- or completely-wetted as depicted in Figure 10 [53].

When encountering surface wetting, the liquid-vapour interphase can be found deeper in the membrane pores in comparison to a non-wetted membrane. This will cause the permeate flux to slowly decrease as the effect of temperature polarization tends to rise, thereby decreasing the temperature at the evaporation interface [54]. It must be noted that in some cases, a momentarily increase in flux was detected due to the shorter path by which the vapours must travel to reach the permeate side [53].

When regarding partially wetted membranes, the feed solution is allowed to enter the pores even further than with surface wetting. This can in some pores even cause complete wetting with the formation of solvent bridges. As long as this is not the case for the majority of the pores, the working of the MD process can still be guaranteed although it leads to a reduction in permeate flux since the amount of evaporation surface drastically decreases (solid blue line, Figure 10), or an increase in flux due to the liquid mass transport by the solvent bridges (blue dash line, Figure 10). Both of these will worsen the separation efficiency of the MD process and must therefore be avoided [52], [55].

For the completely- or fully-wetted membrane, the separation process fails as all liquid is allowed to pass through the membrane pores as is shown by the rejection curve in Figure 10.

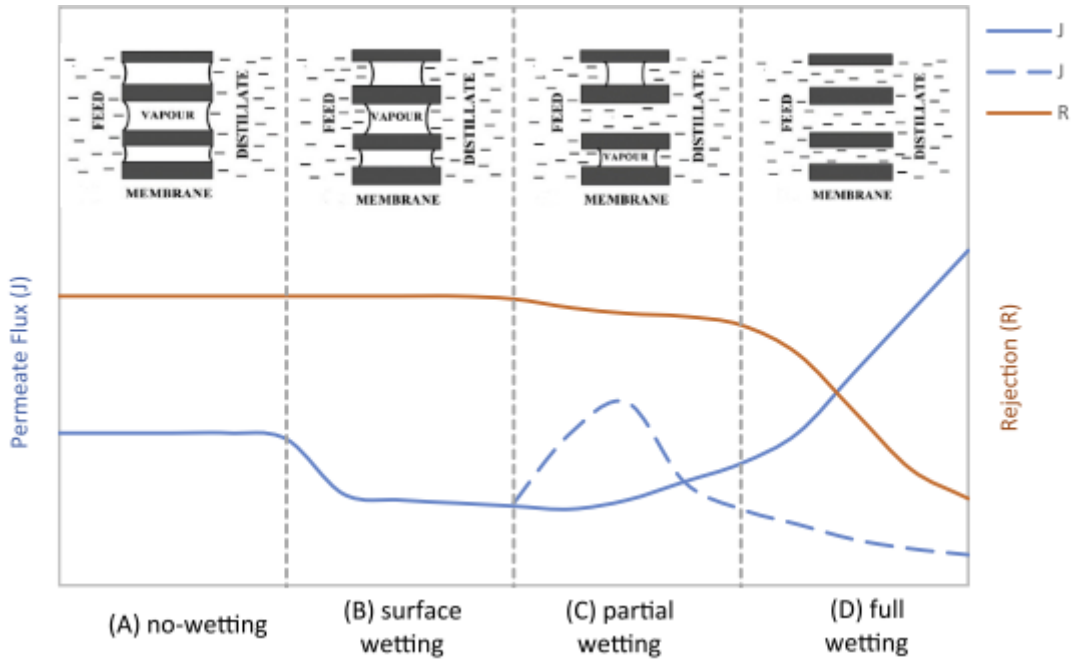

Figure 10: Depiction of flux and rejection degree for each type of wetted state: (A) non-wetted; (B) surface-wetted; (C) partially-wetted; and (D) completely-wetted [52]

2.5.2. Liquid entry pressure

The liquid entry pressure (LEP) is a critical threshold for the transmembrane pressure difference to avoid pore wetting. In theory, as long as this boundary is not overstepped, the feed solution should be prevented from being pushed through the dry membrane pores. Initially, the Young-Laplace equation (Eq. 11) defined the LEP as follows [45]:

$$LEP = \frac{-2\beta\gamma_L \cos\theta}{r_{max}} > P_r - P_p = \Delta P_{interface} \quad (11)$$

Where P_r and P_p represent the hydraulic pressure of the retentate and permeate respectively, γ_L the liquid surface tension [Nm^{-1}], θ the contact angle [°], r_{max} the maximum pore radius [m] and β represents the pore geometry coefficient. It is worth mentioning that the pore geometry coefficient, which serves as a correction factor for irregularly shaped pores, was initially not described within the Young-Laplace equation as the membrane pores were assumed to have a perfect cylindrical shape. So far, a couple of estimations have been given for different pore geometries, which are displayed in Table 5.

Table 5: Pore geometry coefficient (β) for different pore shapes [52]

Pore shape	β-coefficient
Cylindrical pores	1.0
Elliptical or irregularly shaped pores	smaller than 1.0
Stretched membranes (e.g., PTFE) with a small curvature radius	0.4-0.6

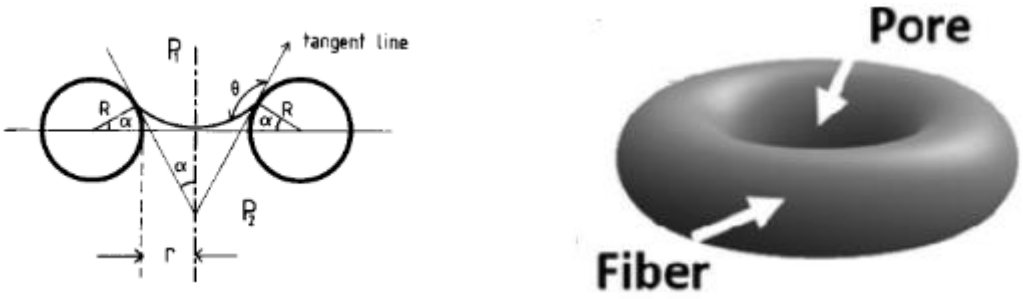

Figure 11: Vapour-liquid interface at pore entrance (left) and donut-like geometry (right) [10], [52]

Unfortunately, merely adding a pore geometry coefficient does not resolve the issue around low contact angles (i.e. contact angles below 90° result in a negative LEP-value), nor does it fully address irregular pore shapes. Therefore, Kim and Herriott proposed an alternative correlation (Eq. 12) in which they assumed the pore entrance to have a donut-like geometry (Figure 11) [10], [56]:

$$LEP = \frac{-2\gamma_L \cos(\theta - \alpha)}{r(1 + (R/r)(1 - \cos\alpha))} \quad (12)$$

where R represents the fibre radius, r is the smallest pore radius and α is the so-called correction angle (all shown in Figure 11). This correction angle can be derived from the contact angle, using equation 13 [10]:

$$\sin(\theta - \alpha) = \frac{(R/r)\sin\theta}{1 + (R/r)} \tag{13}$$

Although this model has provided decent results for liquid-air systems, the deviations for liquid-liquid systems have been substantial and was therefore addressed by Smolders and Franken (1988), Zha et al. (1992) and Hereijgers et al. (2016). The latter one proposed an alteration of the Young-Laplace equation using two different fitting parameters α and β [13]:

$$LEP = \frac{-2\gamma_L \beta \cos(\theta + \alpha)}{r_{max}} \tag{14}$$

This correlation was evaluated with liquid-liquid experiments (containing a wetting liquid at the permeate side and a non-wetting liquid at the retentate side) and proved to be a better fit in comparison to the other models. It decreased the average deviation to 25.0%, which is a slight improvement in comparison to the Zha et al. model (but is far less complicated) and is an improvement of over 10% of the original Young-Laplace equation. Below, a summary is given of all their data for both the liquid-air (Table 6) and the liquid-liquid experiments (Table 7), which will later be used for data comparison.

Table 6: Summary of LEP results for liquid-vapour experiments

Mixture	concentration	LEP	Membrane	Source
Water	-	12.0 psi	PTFE	[10]
Ethylene glycol	-	6.0 psi	PTFE	
Ethanol-water	17 vol%	6.2 psi	PTFE	
	23 vol%	5.5 psi	PTFE	
	33 vol%	4.5 psi	PTFE	
	50 vol%	3.0 psi	PTFE	
	67 vol%	2.5 psi	PTFE	
Acetic acid-water	10 vol%	7.4 psi	PTFE	
	20 vol%	6.0 psi	PTFE	
	30 vol%	5.0 psi	PTFE	
	50 vol%	4.4 psi	PTFE	
n-Heptane	-	108 kPa	PP	[12]
n-Dodecane	-	117 kPa	PP	
Toluene	-	151 kPa	PP	
Kerosene	-	128 kPa	PP	
Shellsol	-	125 kPa	PP	
Ethanol-water	10 %	196 kPa	PP	
	25 %	124 kPa	PP	
n-Heptane	-	215 kPa	PP	[12]
n-Dodecane	-	307 kPa	PP	
Toluene	-	333 kPa	PP	
Kerosene	-	313 kPa	PP	
Shellsol	-	356 kPa	PP	
Ethanol-water	10 %	363 kPa	PP	
	25 %	194 kPa	PP	
n-Heptane	-	65.0 kPa	PVDF	[12]
n-Dodecane	-	78.8 kPa	PVDF	
Toluene	-	84.3 kPa	PVDF	
Kerosene	-	82.6 kPa	PVDF	
Shellsol	-	80.7 kPa	PVDF	
Ethanol-water	10 %	78.9 kPa	PVDF	
	25 %	24.9 kPa	PVDF	
water	-	151 kPa	PVDF	

Table 7: Summary of LEP results for liquid-liquid experiments

Solvent 1	Solvent 2	LEP	Membrane	Source
Water	CCl_4	3.1 psi	PTFE	
Water	n-Hexane	3.1 psi	PTFE	[10]
Water	n-Octane	3.0 psi	PTFE	
Water	MIBK	2.7 psi	PTFE	[10]
Acetic acid-water 10 vol%	MIBK	1.7 psi	PTFE	
Acetic acid-water 20 vol%	MIBK	1.5 psi	PTFE	[10]
Acetic acid-water 30 vol%	MIBK	1.2 psi	PTFE	
Acetic acid-water 50 vol%	MIBK	0.8 psi	PTFE	
Ethanol-water 17 vol%	MIBK	1.6 psi	PTFE	
Ethanol-water 23 vol%	MIBK	1.2 psi	PTFE	[10]
Ethanol-water 33 vol%	MIBK	1.0 psi	PTFE	
Ethanol-water 50 vol%	MIBK	0.8 psi	PTFE	
Water	n-Octanol	50.2 kPa	PP	
Water	n-Heptane	243 kPa	PP	
Water	n-Dodecane	248 kPa	PP	[12]
Water	Toluene	177 kPa	PP	
Water	Kerosene	186 kPa	PP	
Water	Shellsol	202 kPa	PP	
Water	n-Octanol	125 kPa	PP	
Water	n-Heptane	548 kPa	PP	
Water	n-Dodecane	566 kPa	PP	[12]
Water	Kerosene	401 kPa	PP	
Water	Shellsol	430 kPa	PP	
Water	n-Octanol	29.6 kPa	PVDF	
Water	n-Heptane	126 kPa	PVDF	
Water	n-Dodecane	122 kPa	PVDF	[12]
Water	Toluene	95.8 kPa	PVDF	
Water	Kerosene	117 kPa	PVDF	
Water	Shellsol	107 kPa	PVDF	
Water	n-Heptane	3.03 bar	PTFE	
Water	1-Octanol	0.59 bar	PTFE	
Water	MIBK	0.74 bar	PTFE	[13]
Water	Ethyl Acetate	0.52 bar	PTFE	
Water	Toluene	2.58 bar	PTFE	
Water	1-Octanol	4.17 bar	PP	
Water	MIBK	4.24 bar	PP	[13]
Water	Ethyl Acetate	1.19 bar	PP	

2.5.2.1. LEP measurement

Overall, there are two different methods for measuring the LEP, either a static or a dynamic measurement. The static method, originally described by Smolders and Franken, utilizes a liquid feed that is in direct contact with the retentate side of the membrane on which a certain pressure is applied. This pressure will then be increased stepwise until (continuous) flow can be detected at the permeate side, indicating that the pressure difference over the membrane has exceeded the LEP threshold [45]. However, in recent years this method is no longer used as research has proven that the measured LEP-values (using a static experiment) often exceed the actual maximal allowable pressure as this method seems to exhibit hysteresis [57].

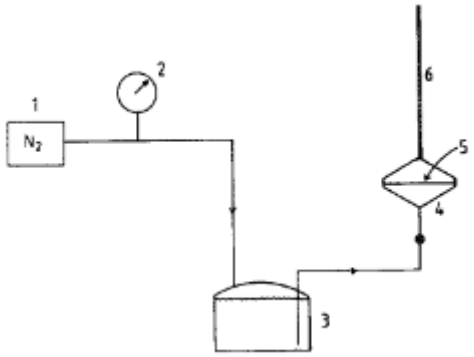

Figure 12: Setup of static LEP measurement, 1= Gas cylinder with nitrogen; 2 = manometer; 3 = liquid feed; 4 = measuring cell; 5 = membrane; 6 = measuring pipette [45]

For the dynamic method, a conventional MD module is utilized in which the feed solution flows by the retentate side of the module. Just as with the static method, the pressure is stepwise increased over time but, in contrast to the static method, it is increased by increasing the feed flow rate. Once flow can be perceived at the permeate side, the LEP threshold is considered to be overstepped. More recent, Warsinger et al. proposed a new method for determining the LEP. They proposed that, once breakthrough occurred, the pressure within the retentate chamber would decrease due to flow escaping through the membrane pored. Based upon their theory, they defined that (once the pressure reached its designated value) the LEP could be found where the stability slope was below just below zero [52].

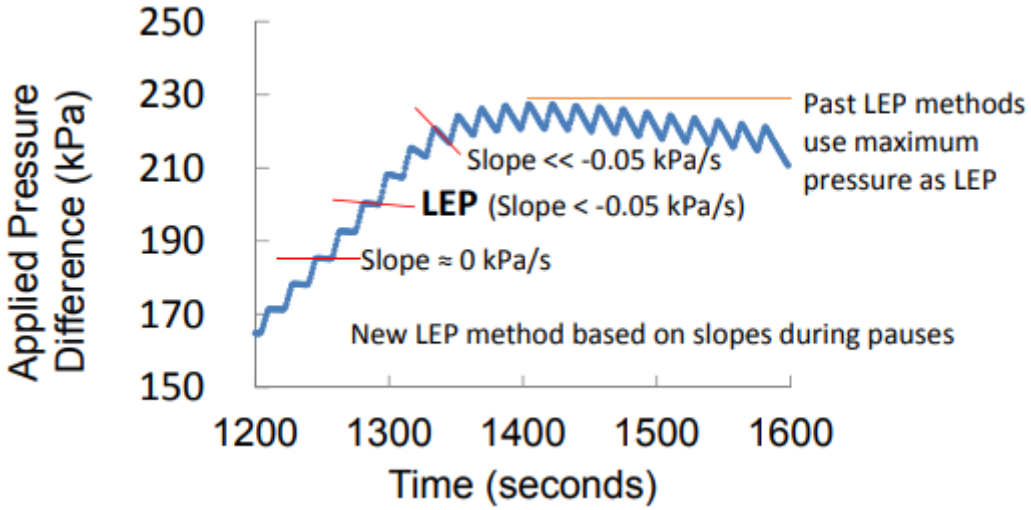

Figure 13: Warsinger method of determining the LEP [52]

2.6. Conclusion

So far, a couple of correlations have been proposed for predicting the LEP, of which the most accurate has been presented by Hereijgers et al. (2015). They achieved an average deviation of 25.0%, using two different fitting parameters as an addition to the Young-Laplace equation. Although this is (so far) the best correlation found within the literature, its accuracy is far from perfect along with the fact that almost no membrane properties are included. In this research, the accuracy of their equation will be tackled by evaluating a couple of influential parameters for aqueous solutions (containing an organic

component) such as the contact angle, surface tension, concentration and polarity. To determine the LEP, a conventional dynamic measurement will be used as the membrane contactor does not allow high flowrates due to its size. The absence of these high flowrates prevent a quick build-up in pressure, which in turn prevents the possibility of using the Warsinger method for these applications.

3. Materials and methods

This chapter is divided into two different sections, one about the correlation for the liquid entry pressure (LEP) and the other about vacuum membrane distillation (VMD).

3.1. Liquid entry pressure correlation

As discussed within the literature study, the most generally used parameters for estimating the LEP are the surface tension and the contact angle. Within this study, LEPs, surface tensions and contact angles were measured for five aqueous solutions, each containing a different miscible organic component (Table 8). For each mixture, different concentrations (i.e. 5, 15, 30, 45 and 60 mol%, regarding the organic component) were prepared and measured. This data, after the addition of the Kamlet-Taft polarity parameter which was retrieved from the literature, was then used for correlation building, using Eureqa software. It is worth mentioning that, before the Eureqa software could be utilized, both the contact angle and the surface tension data were determined by interpolation at the concentrations used for the LEP (as two different sets of solutions with slightly different concentrations were used). All of these interpolations were performed based on the curve fittings retrieved from MATLAB (Appendix A), which generated a correlation for each solvent mixture individually.

Table 8: List of products used for all of the correlation experiments

Product	Purity	Supplier	Cas nr.
Methanol	Hipersolv chromanorm	VWR	67-56-1
Ethanol, absolute	99.8%	Fisher Scientific	64-17-5
Acetic acid glacial	Analar normapur	VWR	64-19-7
Acetone	suprasolv	Merck	67-64-1
Acetonitrile	hypergrade for LC-MS	Merck	75-05-8

3.1.1.Surface tension

The surface tension of the aqueous solutions was determined with an Attension Theta Lite (Biolin Scientific, Figure 14 left image) following the pendant drop principle. A droplet was slowly extruded from a hanging syringe by hand, until the point where the droplet fell of the needle. The shape of the droplet (right before it detached) was then captured by the camera, which allowed the software to find the best curve fitting (following the Young-Laplace equation, Figure 14 right image) around the edges of the droplet. This, in combination with the density of the solution (measured beforehand with the use of a pycnometer, calibrated volume of 49.438 cm^3), yielded a value for the surface tension.

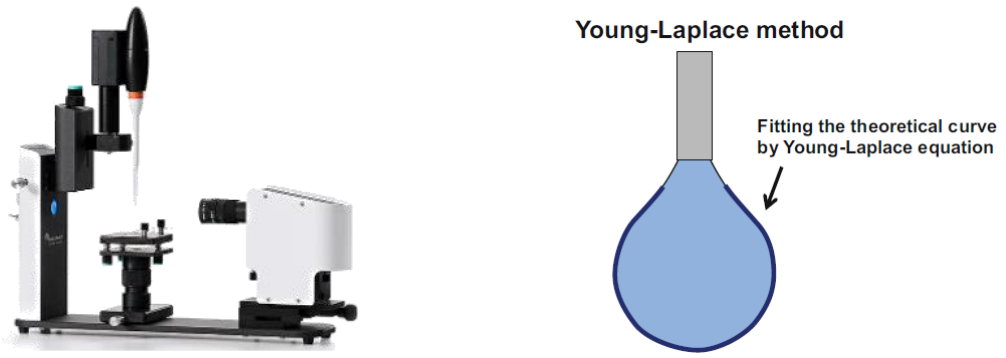

Figure 14: Biolin Scientific Theta Lite (left), Young-Laplace fitting (right) [58], [59]

Since most mixtures (Table 9) contained a volatile organic component (VOC), the surface tension tended to change over time due to evaporation. Therefore, all measurements were repeated five times to ensure that the measurements were reliable. It is also worth mentioning that, in between experiments, the syringe was rinsed five times with milliQ water and afterwards three times with the solution itself before a measurement was performed.

Table 9: Mixtures and their concentration used for surface tension and contact angle measurements

Mixture	Volume (mL)	$Mass_{OC}$ (g)	$Mass_{water}$ (g)	Concentration (mol%)	Measured for …	
					γ_L	θ
methanol-water	200.0	18.9	177.4	5.7%	×	✓
	100.0	23.2	71.9	15.4%	✓	✓
	100.0	38.8	52.8	29.2%	✓	✓
	100.0	51.2	37.7	43.3%	✓	✓
	100.0	61.0	25.2	57.7%	✓	✓
ethanol-water	200.0	23.8	170.6	5.2%	×	✓
	100.0	28.7	65.5	14.6%	✓	✓
	100.0	45.8	44.0	28.9%	✓	✓
	100.0	57.2	30.2	42.6%	✓	✓
	100.0	65.4	18.7	57.8%	✓	✓
acetic acid-water	250.0	38.1	215.4	5.0%	×	✓
	100.0	39.9	65.3	15.5%	✓	✓
	100.0	62.0	44.4	29.5%	✓	✓
	100.0	76.8	30.1	43.4%	✓	✓
	100.0	87.0	20.0	56.6%	✓	✓
acetone-water	250.0	35.6	208.0	5.0%	×	✓
	100.0	35.1	58.7	15.6%	✓	✓
	100.0	51.5	38.4	29.4%	✓	✓
	100.0	63.0	24.4	44.5%	✓	✓
	100.0	68.6	15.9	57.2%	✓	✓
acetonitrile-water	250.0	28.6	214.8	5.5%	×	✓
	100.0	27.4	67.1	15.2%	✓	✓
	100.0	45.0	45.2	30.4%	✓	✓
	100.0	56.7	29.8	45.5%	✓	✓
	100.0	66.7	17.0	63.3%	✓	✓

γ_L: surface tension, θ: contact angle, ×: sample not measured, ✓: sample measured

3.1.2. Contact angle

The contact angles were determined with an Optical Contact Angle (OCA, Dataphysics, Figure 15 left image) which used a pinned down PTFE membrane (Advantec T010A304D, the same that was used during LEP and VMD experiments) as the solid phase upon which 5 µl droplet was placed. As additional tensions can remain when placing the droplet, which alters the measured contact angle, an extra 2 µl is added to ensure the actual contact angle is captured. Just as with the surface tension, a fitting over the shape of the droplet is determined (resulting in the measured contact angle using an elliptical fitting) but also these angles are not consistent over time (due to the evaporation of the VOC) so replicates of this experiment were measured for reliability.

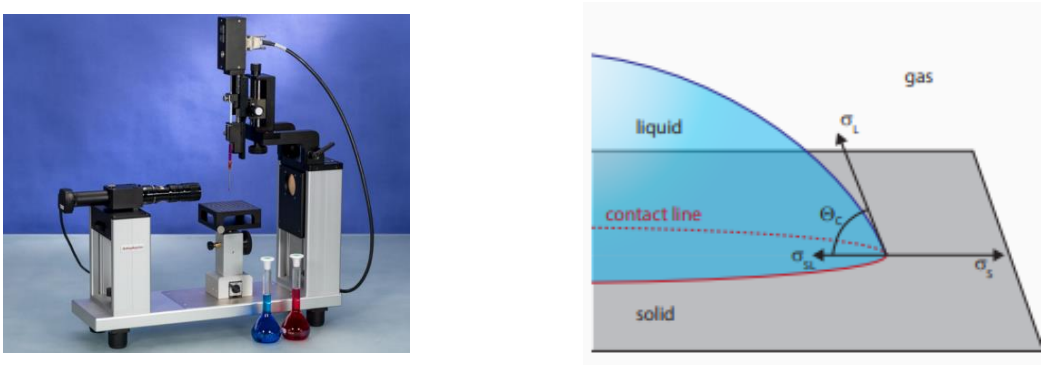

Figure 15: OCA 15EC (left) and schematic of the contact angle (right) [60], [61]

As to address the roughness of the PTFE surface, which alters the measured contact angle, the contact angle was also measured for the 5 mol% methanol and ethanol mixtures on top of PTFE tape (Bonfix, class 0.2). Both the Advantec PTFE and the PTFE were analysed for their roughness with a Diavite compact device (resolution of 0.01 µm) as to implement it as a correction factor following equation X [62]:

$$\cos\theta' = r\cos\theta = \frac{r(\gamma_{SG} - \gamma_{SL})}{\gamma_{LG}} \tag{15}$$

where θ' and θ are the apparent and effective contact angle respectively; r is the ratio of the rough surface area over the smooth surface area; γ_{SG}, γ_{SL} and γ_{LG} are the interfacial tensions between gas (G), liquid (L) and solid (S). Furthermore, it must be mentioned that all experiments regarding contact angles and roughness factors were conducted in a temperature-controlled room (24°C) with a relative humidity of 43%.

3.1.3. Liquid entry pressure

To determine the effective LEP, a membrane microcontactor (MMC, Figure 16) consisting of two aluminium plates clamping a PTFE membrane (Advantec T010A304D, pore size 100 nm, thickness 70 µm, porosity 68%) between them was used. At both the retentate and permeate side, designated channels are milled into the aluminium body to ensure uniform distribution of liquid, leaving pillars between the channels to support the membrane. The channels between those pillars stretch over an area that is 51.48 mm long and 10 mm wide while each channel has a depth of 100 µm and a width of 400 µm, resulting in a total volume of 36.6 µl at both sides of the membrane.

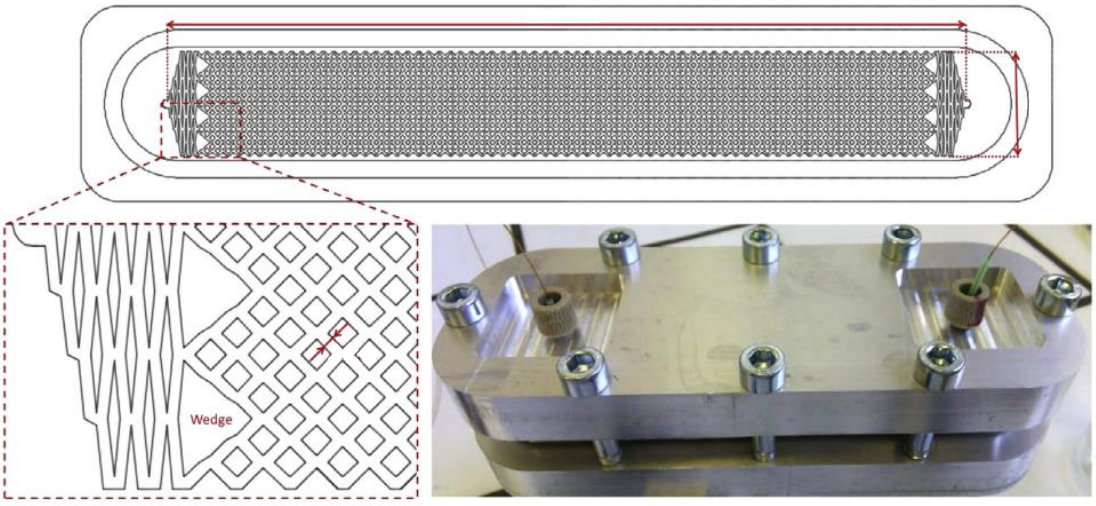

Figure 16: Schematic view of MMC, both on the inside and the outside [5]

As the MMC is kept at 40°C within a heating tub, a Teledyne Isco 500 D syringe pump was used at different flow rates to cause different pressures at the retentate side while the permeate side was left open to the atmosphere. The actual pressure at the retentate side was determined using an Omega pxm319-020g pressure transmitter probe, which was located between the syringe pump and the retentate inlet of the MMC. Because PTFE tubing with an internal diameter of 0.25 mm was used (OD of 1 mm), the pressure drop between the pressure probe and inlet of the contactor could not be neglected and was therefore always measured. This was performed by decoupling the retentate inlet tube from the MMC and then resuming the experiment at the same parameters where breakthrough was detected. The LEP itself was measured using a standard dynamic measurement where the pressure was increased stepwise (each time allowing the pressure to stabilize after increasing the flow rate) until breakthrough, leading to (continuous) flow at the retentate outlet, could be detected.

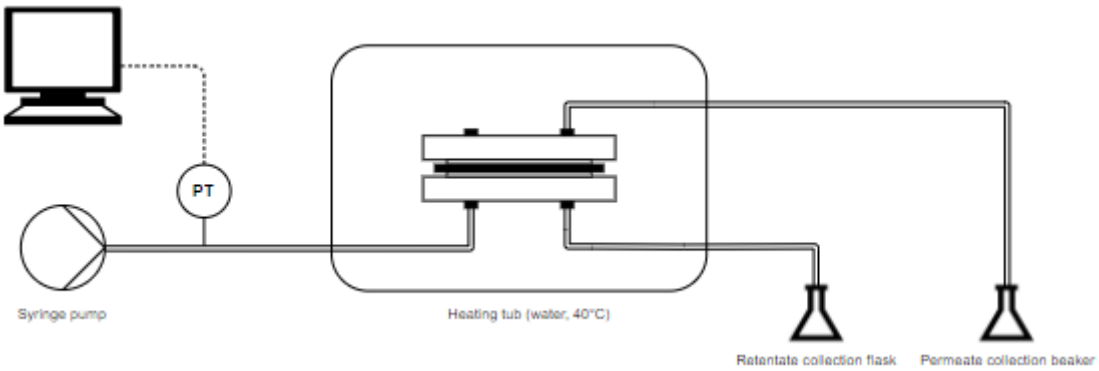

Figure 17: Schematic of experimental setup for LEP determination

As mentioned before, a different set of solutions was used for the LEP determination as was used for the contact angle and surface tension measurements. Their concentration can be found below in Table 10.

Table 10: Mixtures and their concentration used for liquid entry pressure determination

Mixture	Volume (mL)	$Mass_{OC}$ (g)	$Mass_{water}$ (g)	Concentration (mol%)
methanol-water	200.0	18.9	177.4	5.7%
	250.0	56.7	181.6	14.9%
	250.0	98.4	131.7	29.6%
	250.0	130.4	92.8	44.1%
	200.0	123.3	49.6	58.3%
ethanol-water	200.0	23.8	170.6	5.2%
	200.0	58.2	130.5	14.9%
	200.0	93.3	86.0	29.8%
	200.0	116.0	58.5	43.7%
	200.0	131.9	36.6	58.5%
acetic acid-water	250.0	38.1	215.4	5.0%
	200.0	75.6	132.2	14.6%
	200.0	121.6	89.7	28.9%
	200.0	154.1	58.1	44.3%
	200.0	176.1	37.3	58.6%
acetone-water	250.0	35.6	208.0	5.0%
	200.0	67.4	120.7	14.8%
	200.0	101.7	77.7	28.9%
	200.0	122.0	50.7	42.7%
	200.0	136.5	31.6	57.3%
acetonitrile-water	250.0	28.6	214.8	5.5%
	200.0	54.9	133.8	15.3%
	200.0	88.1	91.9	29.6%
	200.0	111.5	62.1	44.1%
	200.0	129.6	38.8	59.5%

3.2. Vacuum membrane distillation

Within the second part of this research, a VMD experiment was performed to evaluate the potential flux and concentrations that can be achieved using the MMC as well as evaluating how the presence of a vacuum at the permeate side impacts the LEP.

3.2.1. Experimental setup

In general, the setup is largely the same as with the setup of the LEP measurements, only the outlet of the permeate side of the MMC and the method of heating were changed. At the permeate outlet, larger tubing (PFA, 1.6 mm ID) was glued to the contactor screw as the original tubing prevented the pump from creating a vacuum inside the contactor due to the narrow inner diameter of the tubing. This PFA tubing was then connected to plasticised PVC tubing (16 mm OD, 10 mm ID) which lead to the first condenser. Using a Lauda thermostat, which was filled with 50-50 glycerol-water (kept at -5°C), most vapour coming through should condense here preventing it to proceed to the vacuum pump. The second condenser was mainly placed out of precaution to prevent any volatile components to escape into the air. Also, an oven from an old GC apparatus was used to

heat the MMC by convection as water was seen leaking into the permeate outlet tube. This of course decreases the actual vacuum within the permeate side even further but ensured no large sample contaminations could occur. Unfortunately, since the first condenser had insufficient cooling, often no sample could be taken there. Therefore, most samples were taken at condenser two which is less reliable as these liquids passed through the vacuum pump, allowing the possibility of losing methanol within the pump's dead space.

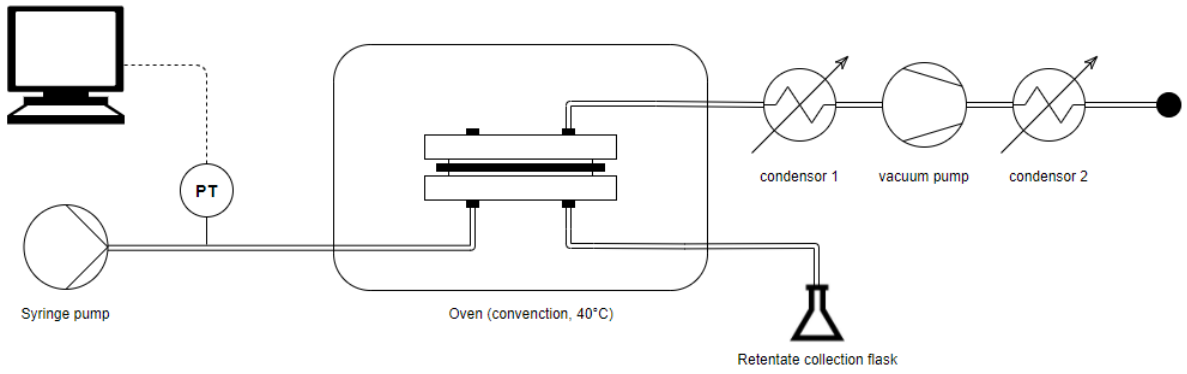

Figure 18: Schematic of the VMD setup

For this experiment, a 44.1 mol% methanol-water mixture was used at flowrates shown in Table 11, corresponding to experimental conditions of the LEP measurements.

Table 11: samples taken at different flowrates during VMD

Flowrate (ml/min)	Retentate sample	Permeate sample
0.1	1R	1P
0.2	2R	2P
0.3	3R	3P
0.4	4R	4P
0.5	5R	5P

3.2.2. VMD sample analysis

The GC samples were prepared by diluting the VMD samples 400 x in 99% pure 1-butanol (Amakem pharmaceutics). Retention times of methanol and butanol are 1.8 and 3.92 minutes, respectively.

All samples taken from the VMD experiment (Table 11) were analysed with an Agilent 6890 series Gas chromatography (GC) apparatus using an FID detector, an HP-5ms column, 5%-phenyl-methylpolysiloxane as stationary phase and nitrogen gas as the mobile phase. 1 µl of each sample was injected into the inlet liner, which was kept at 270°C, during the 12.50-minute lasting experiment at a constant flow. The GC oven ran the following steps for each experiment: at the start of the measurement, the oven was kept at 45°C for 1 minute. Then it heated up at a rate of 10°C per minute until it reached a temperature of 150°C which was maintained for another minute. At this point, the measurement was completed and the oven cooled again until it reached 45°C again. To calculate the concentration of the samples, expressed in ppm, a set of calibration solutions with concentrations ranging from 0 to 1600 ppm were measured, yielding the calibration line below:

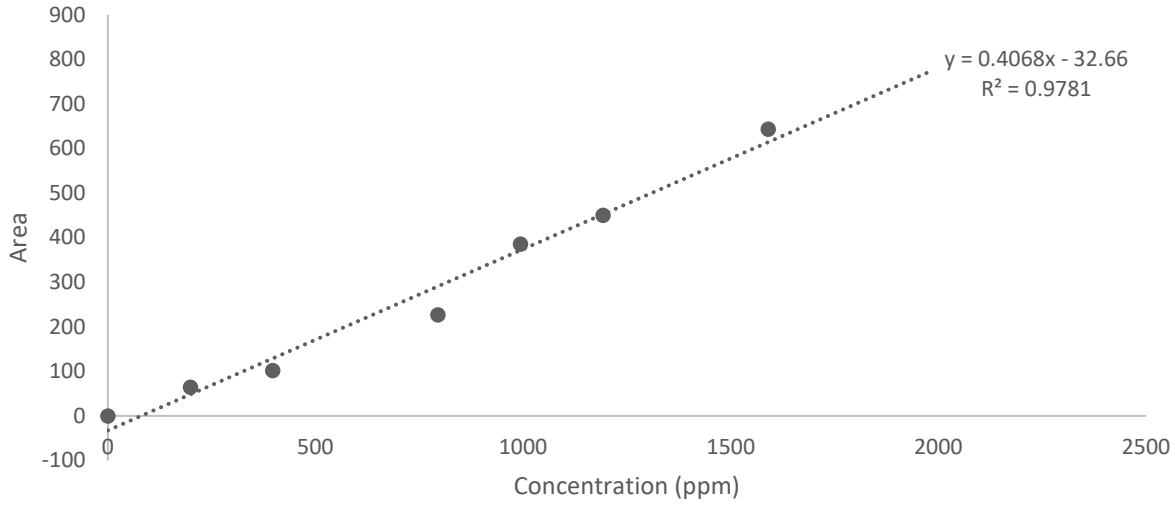

Figure 19: Calibration line for GC-FID analysis

4. Results and discussion

In this chapter, both the results from the measurements leading to the proposed liquid entry pressure (LEP) correlation and the results from the vacuum membrane distillation (VMD) are discussed.

4.1. Liquid entry pressure

For each proposed parameter (i.e. concentration, surface tension, contact angle and Kamlet-Taft polarity) the correlation with the LEP is discussed and a predictive model for LEP based on these parameters is proposed.

4.1.1. Concentration

Figure 20 displays the liquid entry pressure in function of the organic component concentration which shows that increasing the amount of organic solvent causes the LEP to decrease for all solutions except the acetic acid-water solutions. For this specific solution, an initial decrease in LEP was observed until the concentration reached 15 mol% acetic acid. Afterwards, when increasing the concentration even further, the liquid entry pressures tended to increase linearly with the concentration.

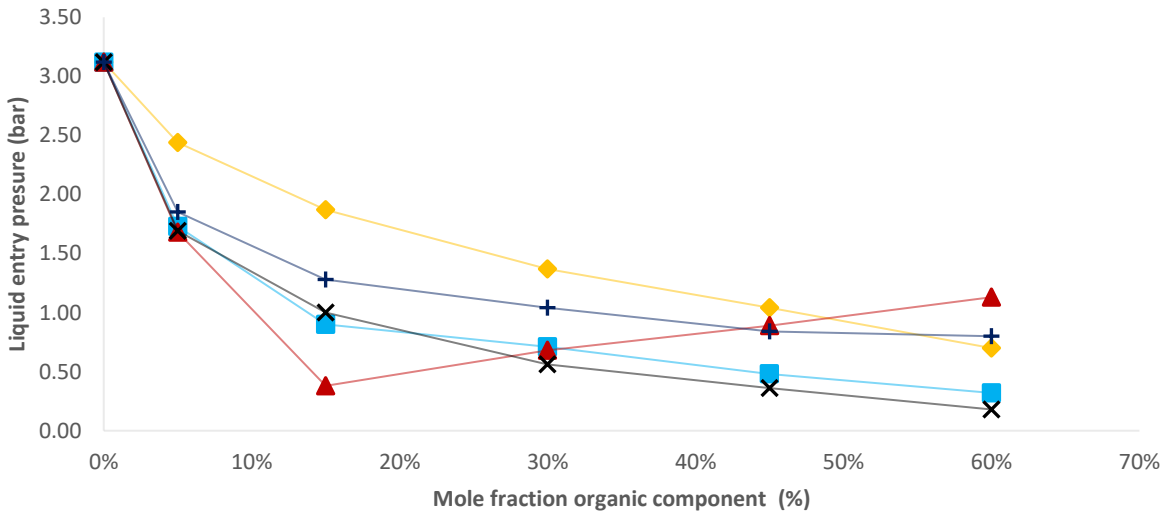

Figure 20: Liquid entry pressure of aqueous mixtures in function of mole fraction of the organic component, methanol-water (◆), ethanol-water (■), acetic acid-water (▲), acetone-water (✕) and acetonitrile-water (✚)

As to address the different behaviour of the acetic acid-water solution, it was compared to the data found by Kim and Harriott [10] who also performed experimental LEP determinations using several different liquid-gas and liquid-liquid experiments (section 2.5.2). From Figure 21 it is clear that, although the measured LEPs for ethanol-water follow a similar trend in comparison to those determined by Kim and Harriott, the acetic acid-water mixture does not show any similarities. They found that increasing the concentration should decrease the LEP. A possible explanation for this different behaviour could be the difference in most volatile component as for acetic acid-water this is water rather than the organic component (boiling point acetic acid at 117.9°C at 1 atm).

However, since the used PTFE membrane has a hydrophobic nature, a decreasing water concentration would simultaneously decrease the polarity of the solution which is expected to decrease the resistance to pore wetting. Because of this unexplained behaviour, the data of acetic acid-water was not used to construct the predictive LEP model.

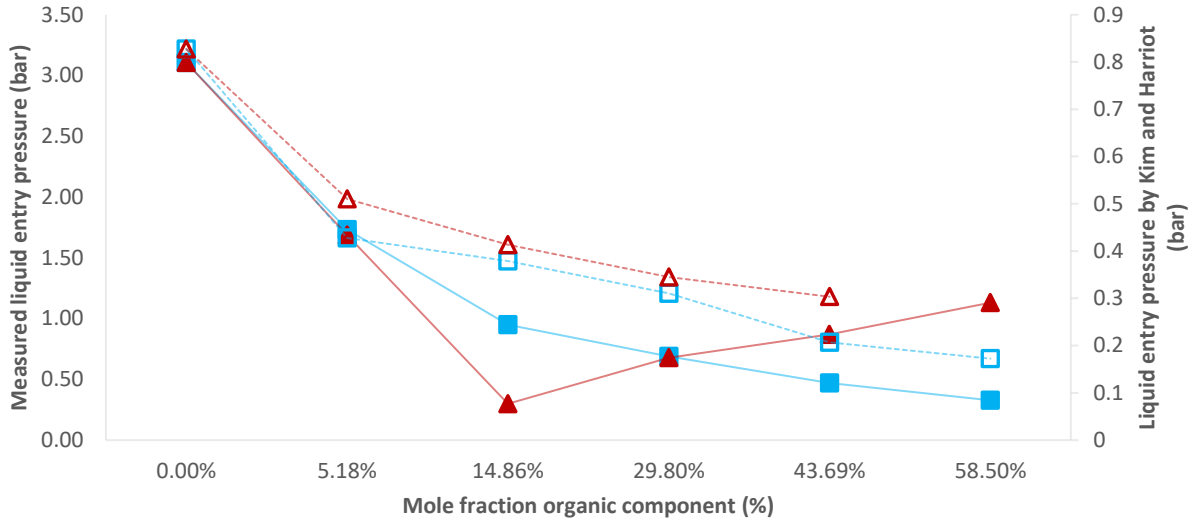

Figure 21: Comparison of measured LEP results to those found by Kim and Harriott [10]*, measured ethanol-water (■) and acetic acid-water (▲), LEP measured for ethanol-water (□) and acetic acid-water (△) by Kim and Harriott*

As to evaluate the impact of the organic component concentration on the LEP, a linear relation was desired to take along in the curve fitting software. The best correlation was found using a negative logarithm of the organic component concentration which showcases an almost perfect linear relation to the LEP, as can be seen in Figure 22. As of the reasons mentioned before, acetic acid-water was no longer included for further data analysis and was therefore left out of the graph below.

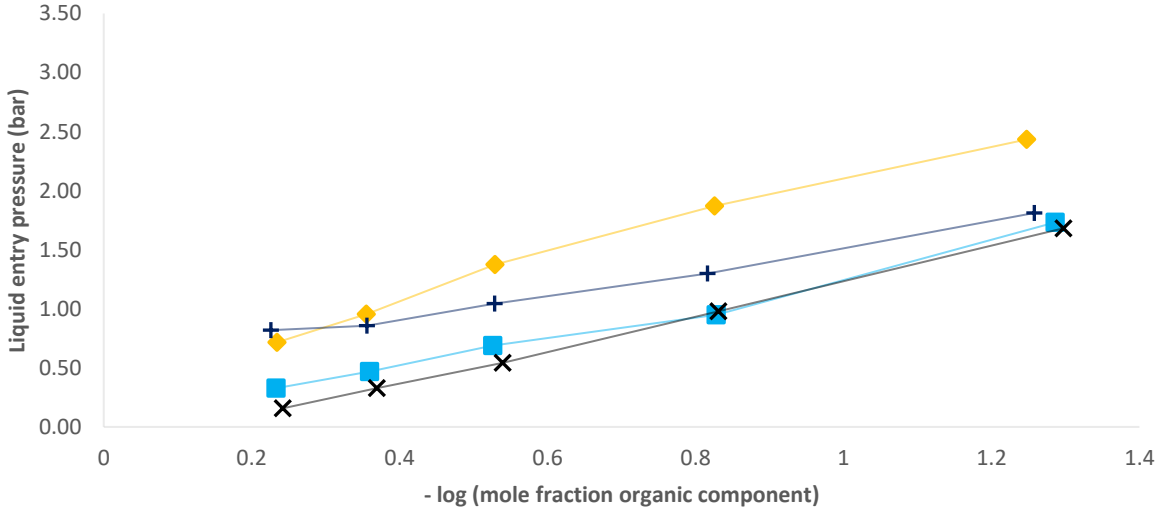

Figure 22: Liquid entry pressure of aqueous mixtures in function of the negative logarithm of their corresponding mole fraction of the organic component, methanol-water (◆), ethanol-water (■), acetone-water (✕) and acetonitrile-water (✚)

4.1.2. Surface tension

In Figure 23 the measured surface tensions are given in function of their corresponding organic component concentration. Increasing the concentration of the organic component causes the surface tension to decrease. It must be mentioned that, although standard deviations were determined during this experiment, they are not displayed in the graph below as they would be unnoticeable (ranged from 0.82 to 0.03).

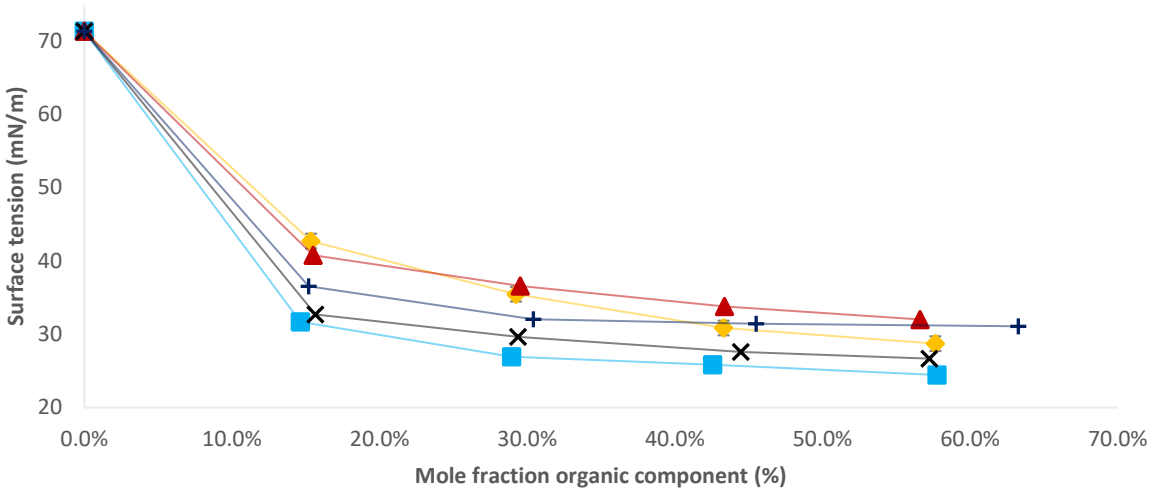

Figure 23; Surface tension of aqueous mixtures in function of mole percentage of the organic component, methanol-water (◆), ethanol-water (■), acetic acid-water (▲), acetone-water (✕) and acetonitrile-water (✚)

This behaviour can be explained by the surface tensions of both solvents, as the surface tension of an ideal binary mixture can theoretically be estimated using the following equation [63]:

$$\sigma_{mix} = \sigma_1 x + \sigma_2 (1 - x) \tag{16}$$

where σ_{mix}, σ_1 and σ_2 represent the surface tension of the mixture, solvent one and solvent two respectively, and x the mole fraction of solvent one. In practice however, the mixture of two solvents will be a non-ideal system causing the relation between the surface tension and mole fraction of the organic component to deviate from their linear relation due to a non-linear relation between the vapour pressure and the composition. Most commonly, a negative deviation from the ideal relation is found (Figure 24) [63].

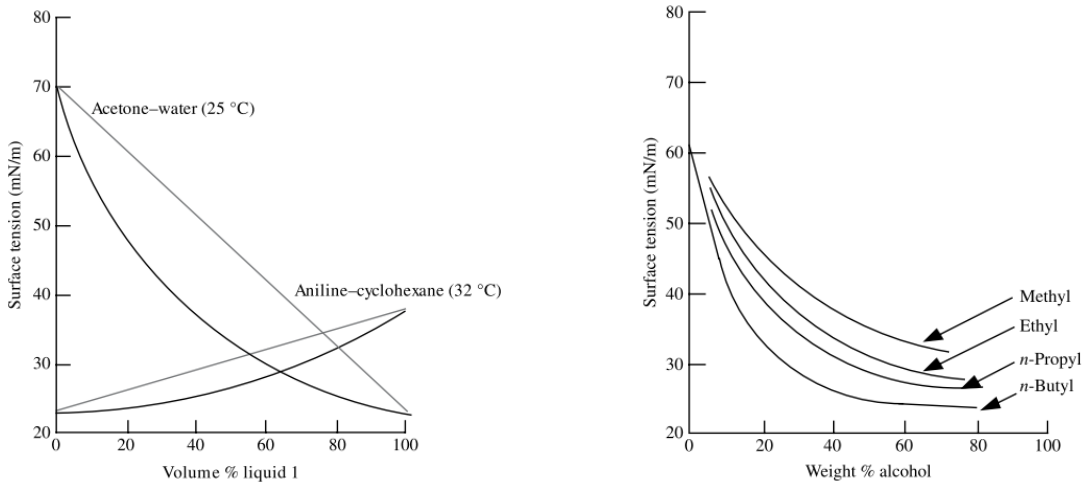

Figure 24: Ideal vs. non-ideal surface tension behaviour (left) and surface tension relation to alcohol weight fraction for different alcohol-water mixtures (right) [63]

When comparing the results from the surface tension measurements to those found within the literature, it is clear that all of the mixtures except acetonitrile-water show great similarity between both data sets. In Figure 25 (left), where methanol-water, ethanol-water and acetic acid-water are shown, it is almost impossible to differentiate the data found in the literature from the results produced in this thesis. This is also the case for the acetone-water mixture, displayed in Figure 25 (right), but not for the acetonitrile-water solution which seems to show no resemblance to the data found in the literature. Since the measured surface tensions of acetonitrile-water seem to resemble the trend of the other mixtures, they likely contained another organic component which would explain the enormous difference between the literature and the resulting data.

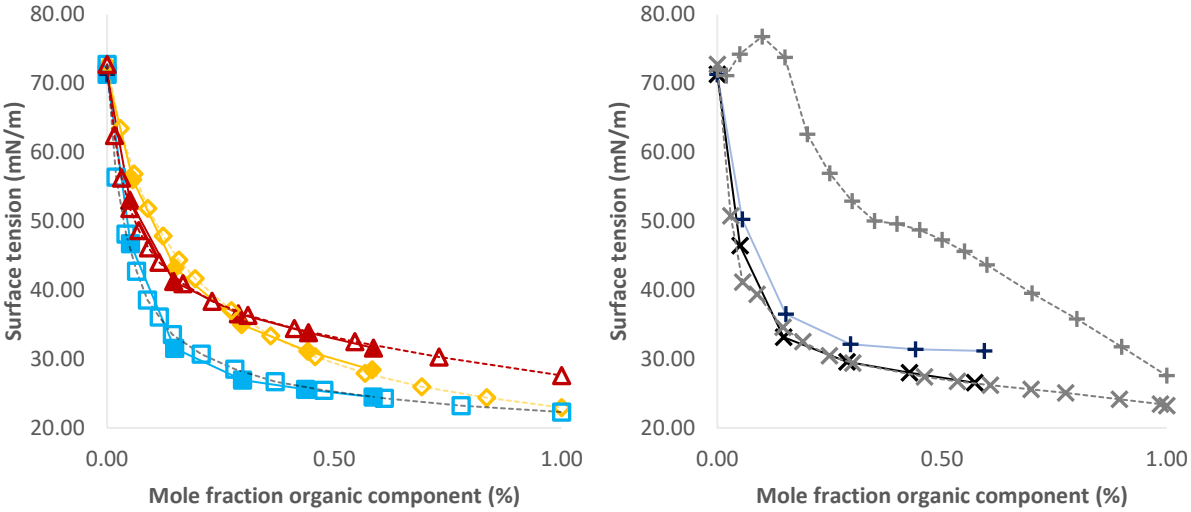

Figure 25: Comparison of measured surface tension results to those available in the literature, measured methanol-water (◆), ethanol-water (■), acetic acid-water (▲), acetone-water (✕) and acetonitrile-water (✚), surface tension data found in literature found for methanol-water [64] *(◇), ethanol-water* [64] *(□) and acetic acid-water* [52] *(△), acetone-water* [65] *(✕) and acetonitrile-water* [52] *(✚)*

Below in Figure 26, the LEP is expressed in function of the surface tension. It shows that mixtures with higher surface tensions yield a higher LEP. Indeed, a larger surface tension indicates a higher water content. And since the PTFE membrane is hydrophobic, a larger water content decreases the wetting of the membrane by the solution.

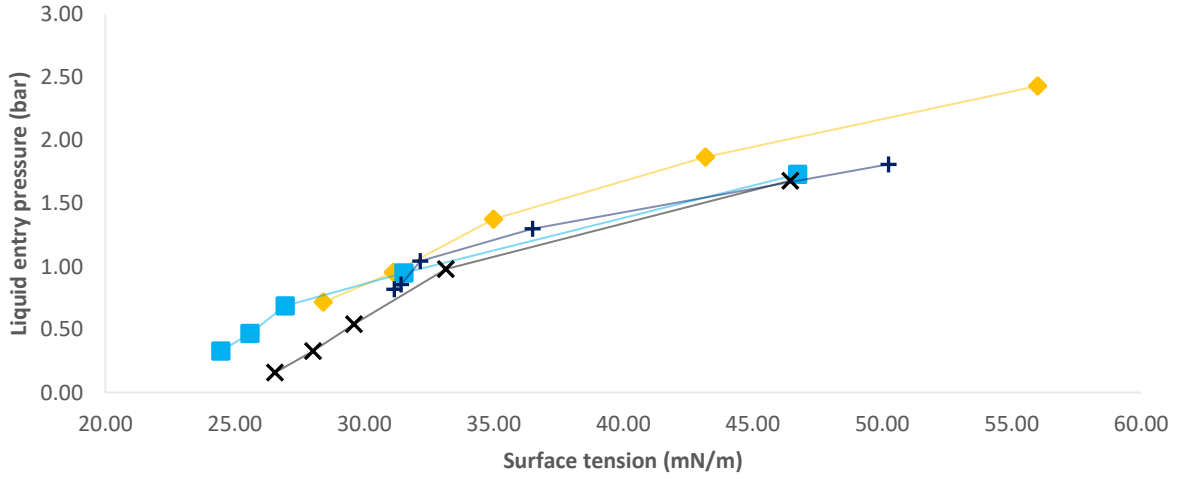

Figure 26: Liquid entry pressure of aqueous mixtures in function of their corresponding surface tension, methanol-water (◆), ethanol-water (■), acetone-water (✕) and acetonitrile-water (✚)

4.1.3. Contact angle

Figure 27 displays the measured contact angles in function of the organic component concentration which shows that increasing the amount of organic solvent causes the contact angle to decrease. This can easily be explained as the membrane is hydrophobic which means that larger contact angles are caused by a larger resistance to wetting. This resistance depends on the affinity between the solution and the membrane which will decrease as the water content in the solution rises resulting in larger contact angles.

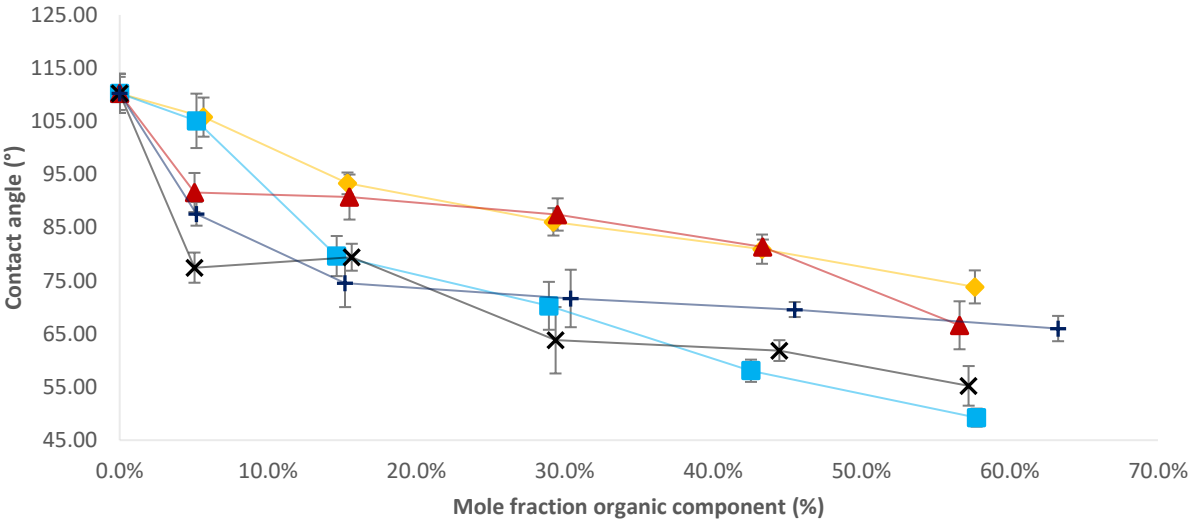

Figure 27; Contact angle of aqueous mixtures in function of mole percentage of the organic component, methanol-water (◆), ethanol-water (■), acetic acid-water (▲), acetone-water (✕) and acetonitrile-water (✚)

When comparing the LEP in function of the contact angle, as is given in Figure 28, it is clear that increasing the contact angles yield a larger maximum allowable pressure. Here again, the hydrophobic nature of the membrane can explain the relationship between both as higher contact angles are the result of a larger water content within the solution which will increase the resistance to wetting.

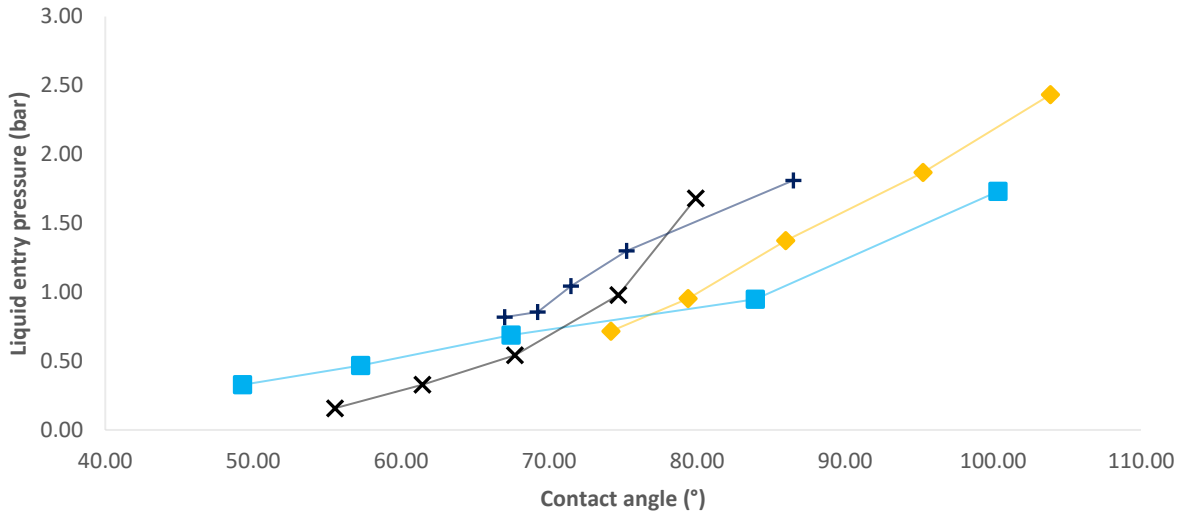

Figure 28: Liquid entry pressure of aqueous mixtures in function contact angle, methanol-water (◆), ethanol-water (■), acetone-water (✕) and acetonitrile-water (✚)

Although the measured contact angles have a clear relation to the LEP, it is sort of common sense to use effective contact angles instead. To acquire the effective contact angle, the measured contact angles should be corrected using the Wenzel equation (section 3.1.2, Eq. 15). Based upon the data from Table 12, no such correction to the contact angles could be made as the Wenzel equation indicates that for hydrophobic solids, the contact angle should increase on a rougher surface [66]. This contradicts the findings from Table 12 which show a decrease in contact angle with increasing surface roughness. A possible explanation for this behaviour could be the porosity of the PTFE Advantec membrane, which will have an additional impact on the measured contact angle.

Table 12: Measured contact angles for different types of PTFE membranes

Mixture	concentration (mol%)	Contact angle (°)	Membrane type	Average roughness (Ra)
Methanol-water	5.653	105.8	PTFE Advantec	0.44
		96.64	PTFE tape	0.72
Ethanol-water	5.175	105.1	PTFE Advantec	0.44
		90.06	PTFE tape	0.72

4.1.4. Kamlet-Taft polarity

The Kamlet-Taft polarity parameter was retrieved from the literature and is taken into consideration for the LEP correlation since organic components often have a lower polarity than water as can be seen in Table 13. Increasing the concentration of these organic components should therefore reduce the polarity of the mixture which could change the interaction with the hydrophobic membrane.

Table 13: Relative polarities of organic solvents and water [67]

Solvent	Relative polarity
acetone	0.355
acetonitrile	0.46
acetic acid	0.648
ethanol	0.654
methanol	0.762
water	1

In Figure 29 the Kamlet-Taft polarity coefficient is plotted in function of the organic component concentration. Although the factor seems to decrease with increasing concentrations, the relation is non-linear and different for each mixture.

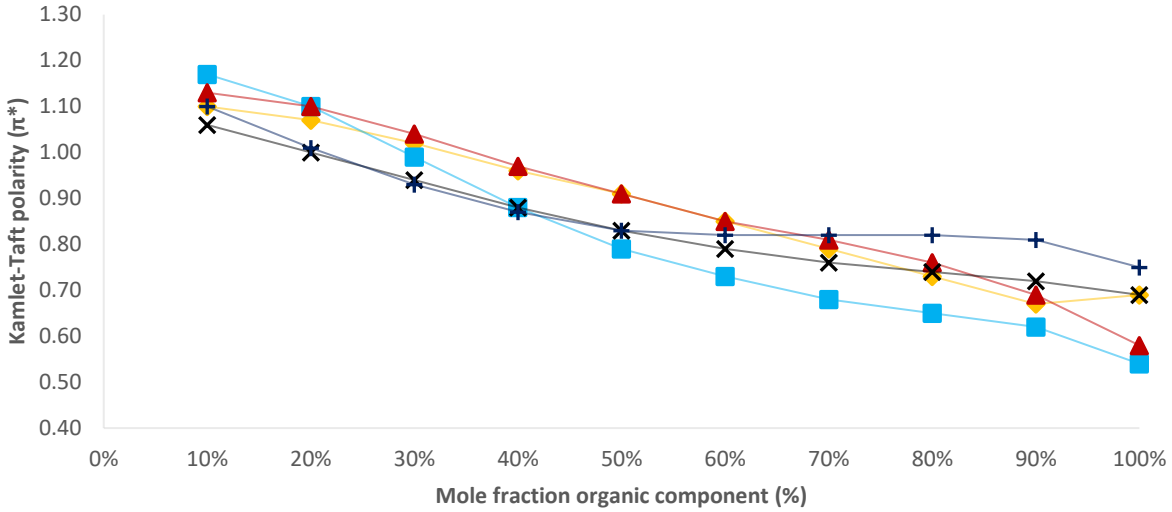

Figure 29: Kamlet-Taft polarity factor in function of concentration [68]*, methanol-water (◆), ethanol-water (■), acetic acid-water (▲), acetone-water (✕) and acetonitrile-water (✚)*

When regarding the LEP in function of the Kamlet-Taft coefficient, Figure 30, it can be observed that the LEP increases with increasing polarity which is to be expected as a larger polarity is caused by having a larger water content in the solution. The remarkable thing however is that for the ethanol-water mixture, two very different LEP were found for two very similar polarities. A possible explanation for this could be that one of the ethanol-water solutions had a concentration that did not correspond well with the used fitting equation (Appendix A), resulting in an over- or underestimation of the actual value.

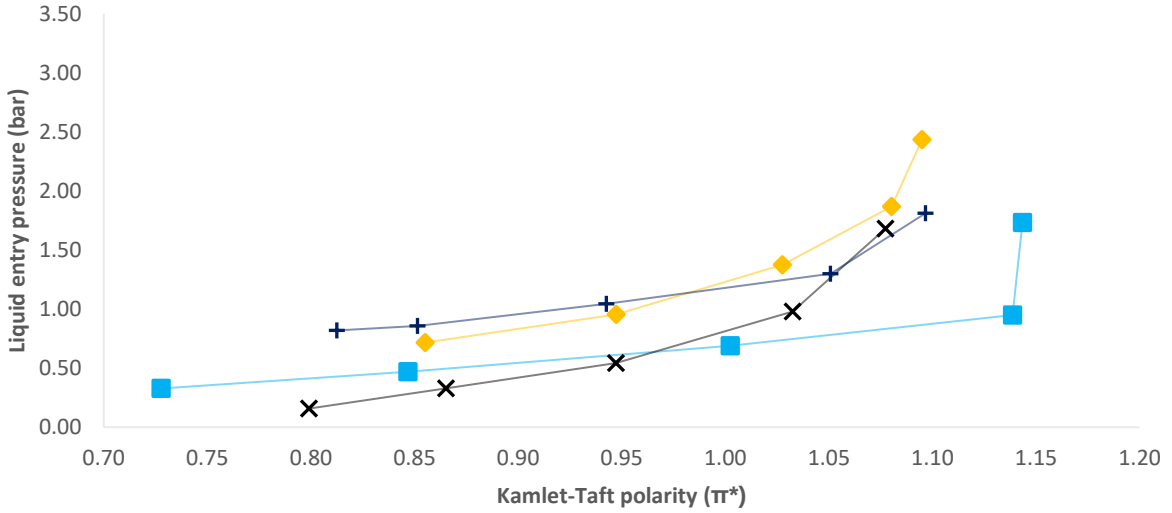

Figure 30: Liquid entry pressure of aqueous mixtures in function of their corresponding Kamlet-Taft factor, methanol-water (◆), ethanol-water (■), acetone-water (✕) and acetonitrile-water (✚)

4.1.5. LEP correlation

After combining the data from all the mixtures (excluding acetonitrile-water and acetic acid-water) and importing it into the fitting software, a couple of different correlations were proposed. Of which the more realistic correlations are given in Table 14:

Table 14: Proposed correlations for the LEP by the Eureqa software

Equation	R^2	Average deviation (%)	Maximum deviation (%)
$LEP = 0.0226\,\gamma_L\,\theta$	0.9423	38.27	267.0
$LEP = 0.0212\,\gamma_L\,\theta\,\pi^*$	0.9604	24.94	176.6
$LEP = -0.0459\,\gamma_L \cos(\theta + 0.937)$	0.9703	24.53	154.5

γ_L: surface tension (mN/m), θ: contact angle (rad), π^*: Kamlet-Taft polarity

As is clear from Table 14, the third equation shows the most resemblance with the used data as it has the largest R^2 along with the lowest average and maximum deviation and is therefore regarded as the best mathematical fit. In addition to that, the equation shows also more resemblance to the previously proposed equations in the literature, in comparison to the other two, as it is the only model to use a negative cosine function of a corrected contact angle. This correction to the contact angle (often represented by α) is a necessity as the effective contact angle within the pores, which should always be above 90° for hydrophobic surfaces, is larger than that measured on the porous membrane surface [66]. All of this leads to the conclusion that the third equation will be the preferable equation to predict the LEP.

When plotting the measured LEPs in function of the predicted LEPs, Figure 31 shows that all data points are in close range of their predicted value except the lower LEP-values of acetone-water, which exceed the 20% error margin (dotted lines). Additionally, the same model seems to show an overestimation for its lower LEP-results while its largest LEP-result has an underestimated LEP value for the proposed model. Both other models also show a deviation from the predicted LEPs, but not as significant as for acetone-water. Nonetheless, the predicted LEP results for all systems seem to be reliable enough to proceed to the proof of concept.

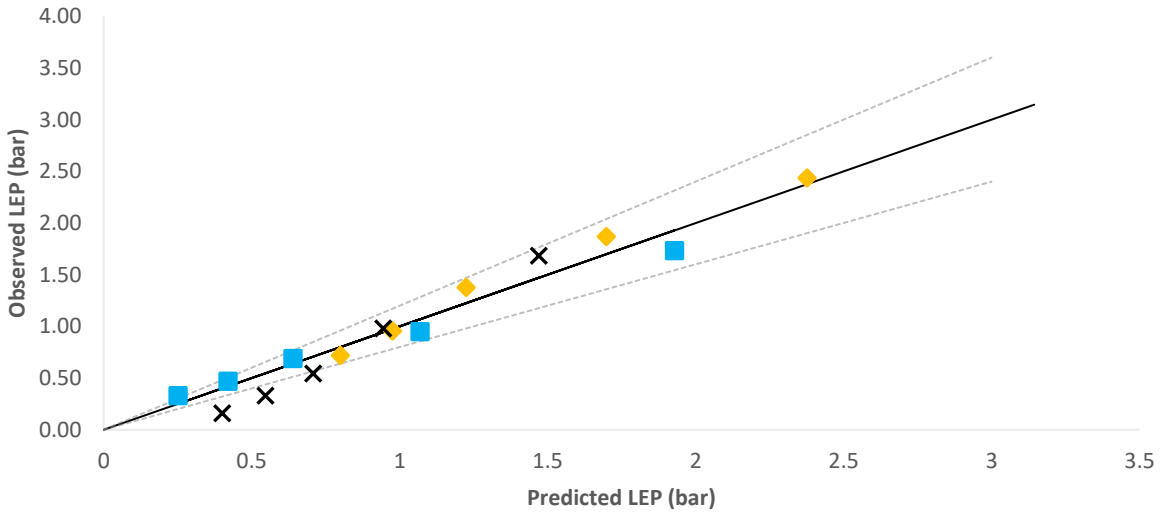

Figure 31: Observed LEP vs. predicted LEP plot, methanol-water (◆), ethanol-water (■) and acetone-water (✕)

Lastly, it must be mentioned that the fitting software did not include the Kamlet-Taft polarity factor and the concentration coefficient into the current correlation. For the concentration, it has clearly been shown that both the contact angle and the surface tension are correlated to the concentration, which was therefore not included as a separate factor in the equation. For the Kamlet-Taft factor, so such correlations were

discovered and its absence is therefore predicted to be due to issues regarding the curve fittings. It could of course be the case that it, just as the concentration, is present in either the contact angle and/or the surface tension but no indication for this was found.

4.1.6. Proof of concept

To evaluate the proposed model, the acetonitrile-water mixture was left out during the fitting exercise and its measured LEP results were later on compared to those predicted by equation 17, both for the measured and literature surface tension. Figure 32 clearly shows that the LEP prediction for the measured surface tensions shows a constant underestimation for all data points while those using the surface tension retrieved from the literature does the opposite. It also seems that the latter set has a larger error margin in comparison to the measured data but none of both displays the desired scatter plot around the prediction line.

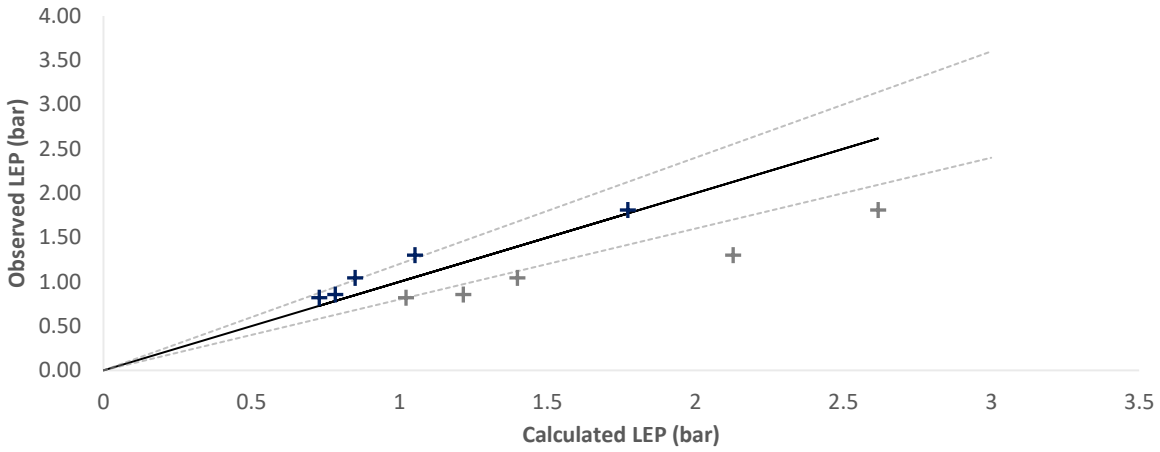

Figure 32: Observed LEP vs. predicted LEP plot for measured acetonitrile-water (✚) and acetonitrile-water with surface tensions retrieved from literature (✚)

As an addition to the proof of concept, the model was also evaluated for the liquid-liquid experiments from Hereijgers et al. (2015) as they used the exact same membrane, which is necessary to compare data as no membrane specific factors were included in the correlation. For the data of the Hereijgers publication, the model seems to give a constant underestimation with an average standard deviation of 26.09%.

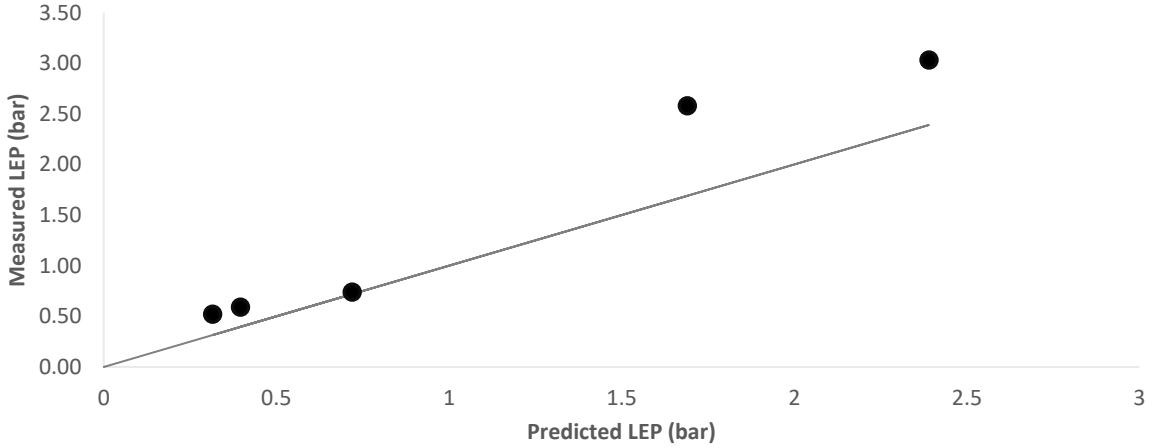

Figure 33: Observed LEP vs. predicted LEP plot for liquid-liquid experiments from Hereijgers et al. [13]

4.2. Vacuum membrane distillation

For the VMD experiment, the results from the GC analysis were discussed as well as the proposed improvements to the experimental setup.

4.2.1.Sample analysis

Figure 34 plots the concentrations of both the permeate and retentate samples in function of their corresponding feed flowrate, with an additional dotted line to indicate the initial feed concentration. Although the retentate samples had a lower concentration than that of the feed solution, which indicates that some methanol was removed while most water was retained at the retentate side of the membrane, the permeate samples displayed concentrations that were below the feed concentration. Normally, when the retentate concentration decreases, the permeate concentration should increase as the volatile component moves through the membrane. therefore, the concentration of the permeate should always be higher than that of the feed. This is clearly not the case here, which is probably because all permeate samples were collected at condenser two, meaning that they passed through the vacuum pump. Inside and at the outlet of that pump, an increased pressure is present which could induce condensation of both methanol and water. This could lead to liquid methanol accumulating inside the pump while still uncondensed water with a minimal concentration of methanol could pass through and get collected at the second condenser, resulting in lower methanol concentrations at the permeate side.

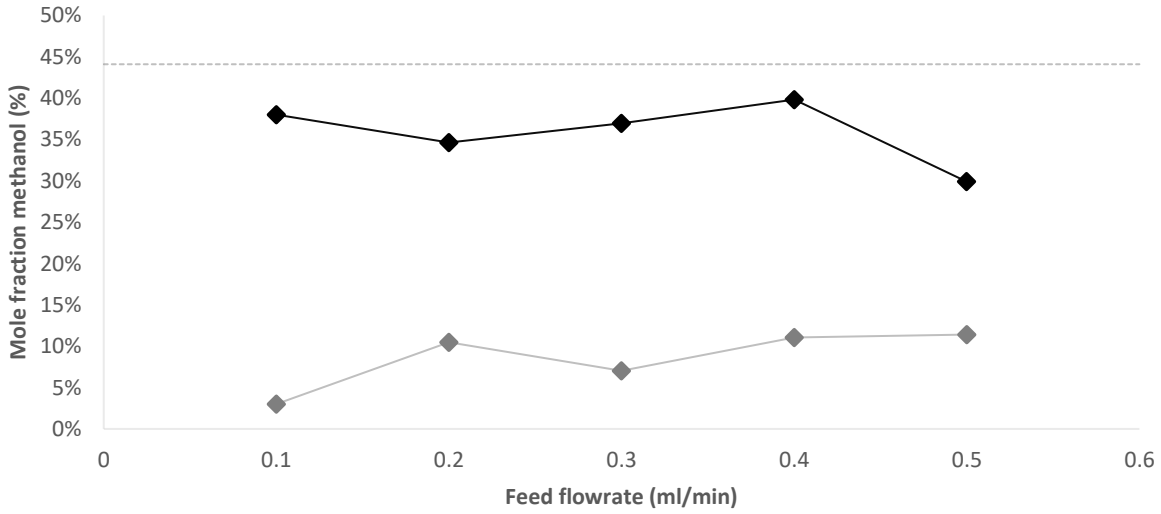

Figure 34: GC-FID results of the methanol concentration in the retentate (◆) and permeate (◆) for a feed solution with 44.1 mol% methanol in water (---)

Another possibility is that no methanol accumulates in the vacuum pump (or is allowed to exit the system through leaks) and that the samples get contaminated with water that is either already present in the condenser or gets drawn in by the vacuum pump through leaks or other connections to the surrounding air. Although it is a possibility, it seems rather unlikely as (based upon the mass balance below, Table 15) the additional water required from the surrounding to achieve such dilutions would be almost as much as the feed flowrate.

Table 15: Mass balances for GC-samples VMD in case of water contamination

Feed flowrate (ml/min)	Permeate concentration (mol%)[a]	Permeate flowrate (ml/min)[b]	Retentate concentration (mol%)[a]	Retentate flowrate (ml/min)[a]	Additional water flowrate (ml/min)[b]
0.1	3.01	0.119	37.99	0.0971	0.116
0.2	10.47	0.155	34.65	0.176	0.131
0.3	7.03	0.288	36.96	0.264	0.252
0.4	11.06	0.200	39.83	0.355	0.155
0.5	11.41	0.464	29.90	0.441	0.405

a: measured parameter, b: calculated based on mass balances

It must also be mentioned that, as this experiment was also assigned to address breakthrough for VMD, no indication was found that the breakthrough occurred as no sudden decrease of the permeate concentration (after increasing the flowrate) was detected.

4.2.2. Proposed improvements to the experimental VMD setup

As is clear from the sample analysis of the VMD experiment, there are still improvements to be made to the experimental setup. The most important are ensuring and measuring the applied vacuum pressure at the permeate side of the membrane, better sample collection and optimizing the sample analysis which are all discussed in this section.

During the VMD experiments, it became clear that vacuum pressure at the permeate side was an uncertainty that was not easily resolved. Using tubing with a diameter of 0.25 mm caused a large resistance, resulting in either a very weak or no vacuum at the membrane of the permeate side. It would therefore be recommended to add a manometer that could indicate the pressure in the contactor, use tubing with larger diameters and use a stronger vacuum pump to decrease the amount of time required to apply the vacuum. Additionally, the internal resistance of the contactor could also be decreased by widening the gaps between the pillars which support the membrane. By doing so, the pressure in the permeate side of the contactor could be more evenly dispersed over the membrane surface resulting in generally higher transmembrane pressure difference.

For the sample collection, the problem is mainly located in the first condenser as the used setup had insufficient cooling to collect any samples. This insufficiency could be resolved by either decreasing the temperature of the cooling or by increasing the residence time. Also, it would be beneficial if a sampler could be connected to the bottom of the cooler to provide the possibility of immediately taking a sample without loss of vacuum pressure. This way, samples can be taken more productively.

Lastly, the analysis method of the methanol-water mixtures should be evaluated. In this research, a GC-FID analysis was used which is rather uncommon for methanol-water solutions as the FID detector does not pick up any water alongside the fact that the samples must be diluted in another solvent as to prevent the water from disturbing the sample evaporation. Generally, the combination of measuring the refractive index and the density is used to evaluate these types of mixtures, as it is a simple method that requires no dilutions or any other type of sample preparations. Unfortunately, no samples were

measured using this method as it was initially viewed as unstable due to fluctuating results caused by temperature changes.

5. Conclusion

As the objective of this research was to evaluate the liquid entry pressure (LEP) for membrane distillation applications, four different parameters were evaluated to address their impact. All parameters were tested using five different aquatic solutions containing a single organic component (i.e. methanol, ethanol, acetic acid, acetone and acetonitrile), to propose a correlation to predict the LEP for a given mixture. Initially, all mixtures except acetonitrile-water were considered as model systems, based upon which the correlation was predicted. The Acetonitrile-water solutions on the other hand were utilized as a proof of concept to evaluate the proposed correlation.

For the concentration, the LEP seemed to decrease as the organic component content increased, for all mixtures except acetic acid. As this contradicted findings within the literature for the acetic acid-mixture, the system was no longer taken into consideration as a model solution. Furthermore, the LEP showed a linear relation with the negative logarithm of the concentration of the organic component.

When regarding the contact angle and the surface tension, a positive relation was found with the LEP. When comparing the measured data of the surface tension to those found in literature, all systems except acetonitrile-water showed great resemblance between both sets. As two different sets were obtained, both could be compared within the proof of concept.

Last, the Kamlet-Taft polarity factor was gathered from the literature. This parameter also showed a positive relation to the LEP and was therefore taken along as a potential factor to predict the LEP.

As the result of the curve fitting, the following equation was proposed:

$$LEP = -0.0459\gamma_L \cos(\theta + 0.937)$$

with γ_L and θ corresponding to the surface tension and the measured contact angle respectively, and a correction angle which is equal to 53.7° or 0.937 rad. This correlation was deemed the best fit with an R^2 of 0.9703 and a maximum deviation of 154.5% and an average deviation of 24.53%. Additionally, when comparing the data from acetonitrile-water to the proposed equation, it was found that the predicted model showed a constant underestimation (no larger than 25%) when using the measured surface tension data. The literature data for the surface tension however, resulted in a constant overestimation with a larger error margin in comparison to the measured surface tensions. Also, as an addition to the proof of concept, experiments by Hereijgers et al. (2015) was compared to the proposed equation resulting in an average deviation of 26.09%.

At the end of the thesis, a vacuum membrane distillation was performed to evaluate how well the membrane microcontactor could perform for such an application. Based on the samples during the experiment, no breakthrough was detected along with a decrease in concentration of the organic component for the permeate samples which indicates the evaporation of the organic component. For the permeate samples, very low

concentrations were measured, indicating that either methanol was escaping the system or water was getting in. The latter seemed less probable after careful analysis of the mass balance. Therefore, a couple of possible improvements were proposed to overcome current issues with the vacuum pressure at the permeate side, sample collection and analytical methods.

References

[1] M. S. El-Bourawi, Z. Ding, R. Ma, and M. Khayet, "A framework for better understanding membrane distillation separation process," *J. Memb. Sci.*, vol. 285, no. 1–2, pp. 4–29, 2006, doi: 10.1016/j.memsci.2006.08.002.

[2] M. Khayet and T. Matsuura, "Introduction to Membrane Distillation," in *Membrane Distillation*, M. Khayet and T. Matsuura, Eds. Amsterdam: Elsevier, 2011, pp. 1–16.

[3] M. Khayet and T. Matsuura, "Vacuum Membrane Distillation," in *Membrane Distillation*, M. Khayet and T. Matsuura, Eds. Amsterdam: Elsevier, 2011, pp. 323–359.

[4] K. W. Lawson and D. R. Lloyd, "Membrane distillation," *J. Memb. Sci.*, vol. 124, no. 1, pp. 1–25, 1997, doi: 10.1016/S0376-7388(96)00236-0.

[5] J. Hereijgers, N. van Oeteren, J. F. M. Denayer, T. Breugelmans, and W. De Malsche, "Multistage counter-current solvent extraction in a flat membrane microcontactor," *Chem. Eng. J.*, vol. 273, pp. 138–146, Aug. 2015, doi: 10.1016/j.cej.2015.03.025.

[6] B. R. Bodell, "Silicone rubber vapor diffusion in saline water distillation," United States Patent Serial No. 185032, 1963.

[7] Q. Zhang *et al.*, "Ethanol production by modified polyvinyl alcohol-immobilized Zymomonas mobilis and in situ membrane distillation under very high gravity condition," *Appl. Energy*, vol. 202, pp. 1–5, Sep. 2017, doi: 10.1016/j.apenergy.2017.05.105.

[8] E. Curcio and E. Drioli, "Membrane distillation and related operations - A review," *Sep. Purif. Rev.*, vol. 34, no. 1, pp. 35–86, 2005, doi: 10.1081/SPM-200054951.

[9] A. C. M. Franken, J. A. M. Nolten, M. H. V. Mulder, D. Bargeman, and C. A. Smolders, "Wetting criteria for the applicability of membrane distillation," *J. Memb. Sci.*, vol. 33, no. 3, pp. 315–328, 1987, doi: 10.1016/S0376-7388(00)80288-4.

[10] B. S. Kim and P. Harriott, "Critical entry pressure for liquids in hydrophobic membranes," *J. Colloid Interface Sci.*, vol. 115, no. 1, pp. 1–8, 1987, doi: 10.1016/0021-9797(87)90002-6.

[11] G. Rácz, S. Kerker, Z. Kovács, G. Vatai, M. Ebrahimi, and P. Czermak, "Theoretical and Experimental Approaches of Liquid Entry Pressure Determination in Membrane Distillation Processes," *Period. Polytech. Chem. Eng.*, vol. 58, no. 2, pp. 81–91, 2014, doi: 10.3311/PPch.2179.

[12] F. F. Zha, A. G. Fane, C. J. D. Fell, and R. W. Schofield, "Critical displacement pressure of a supported liquid membrane," *J. Memb. Sci.*, vol. 75, no. 1–2, pp. 69–80, Dec. 1992, doi: 10.1016/0376-7388(92)80007-7.

[13] J. Hereijgers, T. Breugelmans, and W. De Malsche, "Breakthrough in a flat channel membrane microcontactor," *Chem. Eng. Res. Des.*, vol. 94, pp. 98–104, Feb. 2015, doi: 10.1016/j.cherd.2014.12.004.

[14] M. A. Izquierdo-Gil, "Membrane distillation," in *Separation and Purification Technologies in Biorefineries*, 2013, pp. 301–325.

[15] A. A. Kiss and O. M. Kattan Readi, "An industrial perspective on membrane distillation processes," *J. Chem. Technol. Biotechnol.*, vol. 93, no. 8, pp. 2047–2055, 2018, doi: 10.1002/jctb.5674.

[16] M. Khayet and T. Matsuura, "Future Directions in Membrane Distillation," in *Membrane Distillation*, M. Khayet and T. Matsuura, Eds. Amsterdam: Elsevier, 2011, pp. 453–460.

[17] G. Zaragoza, J. A. Andrés-Mañas, and A. Ruiz-Aguirre, "Commercial scale membrane distillation for solar desalination," *npj Clean Water*, vol. 1, no. 1, pp. 1–6, 2018, doi: 10.1038/s41545-018-0020-z.

[18] M. Reza Shirzad Kebria and A. Rahimpour, "Membrane Distillation: Basics, Advances, and Applications," in *Advances in Membrane Technologies*, A. Abdelrasoul, Ed. IntechOpen, 2020.

[19] A. Alkhudhiri, N. Darwish, and N. Hilal, "Membrane distillation: A comprehensive review," *Desalination*, vol. 287, pp. 2–18, Feb. 2012, doi: 10.1016/j.desal.2011.08.027.

[20] M. Khayet and T. Matsuura, "Direct Contact Membrane Distillation," in *Membrane Distillation*, M. Khayet and T. Matsuura, Eds. Amsterdam: Elsevier, 2011, pp. 249–293.

[21] M. Khayet and T. Matsuura, "Air Gap Membrane Distillation," in *Membrane Distillation*, M. Khayet and T. Matsuura, Eds. Amsterdam: Elsevier, 2011, pp. 361–398.

[22] M. Khayet and T. Matsuura, "Sweeping Gas Membrane Distillation," in *Membrane Distillation*, M. Khayet and T. Matsuura, Eds. Amsterdam: Elsevier, 2011, pp. 295–322.

[23] F. Benyahia, "Membrane Distillation Desalination Principles and Configurations," in *Membrane-Distillation in Desalination*, New York: Taylor& Francis Group, 2019, pp. 19–32.

[24] C. K. Chiam and R. Sarbatly, "Vacuum membrane distillation processes for aqueous solution treatment-A review," *Chem. Eng. Process. - Process Intensif.*, vol. 74, pp. 27–54, 2013, doi: 10.1016/j.cep.2013.10.002.

[25] S. G. Lovineh, M. Asghari, and B. Rajaei, "Numerical simulation and theoretical study on simultaneous

effects of operating parameters in vacuum membrane distillation," *Desalination*, vol. 314, pp. 59–66, 2013, doi: 10.1016/j.desal.2013.01.005.
[26] B. Qi, B. Li, and S. Wang, "Investigation of shell side heat transfer in cross-flow designed vacuum membrane distillation module," *Ind. Eng. Chem. Res.*, vol. 51, no. 35, pp. 11463–11472, 2012, doi: 10.1021/ie203026b.
[27] M. Khayet and T. Matsuura, "Preparation and Characterization of Polyvinylidene Fluoride Membranes for Membrane Distillation," *Ind. Eng. Chem. Res.*, vol. 40, no. 24, pp. 5710–5718, 2001.
[28] F. A. Banat and J. Simandl, "Removal of benzene traces from contaminated water by vacuum membrane distillation," *Chem. Eng. Sci.*, vol. 51, no. 8, pp. 1257–1265, 1996, doi: 10.1016/0009-2509(95)00365-7.
[29] A. M. Alklaibi and N. Lior, "Membrane-distillation desalination: Status and potential," *Desalination*, vol. 171, no. 2, pp. 111–131, 2005, doi: 10.1016/j.desal.2004.03.024.
[30] L. Martínez-Díez and M. I. Vázquez-González, "Temperature and concentration polarization in membrane distillation of aqueous salt solutions," *J. Memb. Sci.*, vol. 156, no. 2, pp. 265–273, 1999, doi: 10.1016/S0376-7388(98)00349-4.
[31] R. W. Schofield, A. G. Fane, C. J. D. Fell, and R. Macoun, "Factors affecting flux in membrane distillation," *Desalination*, vol. 77, no. C, pp. 279–294, 1990, doi: 10.1016/0011-9164(90)85030-E.
[32] F. A. Banat and J. Simandl, "Membrane distillation for dilute ethanol: Separation from aqueous streams," *J. Memb. Sci.*, vol. 163, no. 2, pp. 333–348, 1999, doi: 10.1016/S0376-7388(99)00178-7.
[33] F. A. Banat and J. Simandl, "Theoretical and experimental study in membrane distillation," *Desalination*, vol. 95, no. 1, pp. 39–52, 1994, doi: 10.1016/0011-9164(94)00005-0.
[34] M. C. García-Payo, M. A. Izquierdo-Gil, and C. Fernández-Pineda, "Air gap membrane distillation of aqueous alcohol solutions," *J. Memb. Sci.*, vol. 169, no. 1, pp. 61–80, 2000, doi: 10.1016/S0376-7388(99)00326-9.
[35] K. W. Lawson and D. R. Lloyd, "Membrane distillation. I. Module design and performance evaluation using vacuum membrane distillation," *J. Memb. Sci.*, vol. 120, no. 1, pp. 111–121, 1996, doi: 10.1016/0376-7388(96)00140-8.
[36] M. A. Izquierdo-Gil, M. C. García-Payo, and C. Fernández-Pineda, "Air gap membrane distillation of sucrose aqueous solutions," *J. Memb. Sci.*, vol. 155, no. 2, pp. 291–307, 1999, doi: 10.1016/S0376-7388(98)00323-8.
[37] J. M. Li *et al.*, "Microporous polypropylene and polyethylene hollow fiber membranes. Part 3. Experimental studies on membrane distillation for desalination," *Desalination*, vol. 155, no. 2, pp. 153–156, 2003, doi: 10.1016/S0011-9164(03)00292-3.
[38] K. W. Lawson and D. R. Lloyd, "Membrane distillation. II. Direct contact MD," *J. Memb. Sci.*, vol. 120, no. 1, pp. 123–133, 1996, doi: 10.1016/0376-7388(96)00141-X.
[39] M. Khayet, P. Godino, and J. I. Mengual, "Theory and experiments on sweeping gas membrane distillation," *J. Memb. Sci.*, vol. 165, no. 2, pp. 261–272, 2000, doi: 10.1016/S0376-7388(99)00236-7.
[40] M. Khayet, M. P. Godino, and J. I. Mengual, "Theoretical and experimental studies on desalination using the sweeping gas membrane distillation method," *Desalination*, vol. 157, no. 1–3, pp. 297–305, 2003, doi: 10.1016/S0011-9164(03)00409-0.
[41] S. Bandini, C. Gostoli, and G. C. Sarti, "Separation efficiency in vacuum membrane distillation," *J. Memb. Sci.*, vol. 73, no. 2–3, pp. 217–229, 1992, doi: 10.1016/0376-7388(92)80131-3.
[42] G. C. Sarti, C. Gostoli, and S. Bandini, "Extraction of organic components from aqueous streams by vacuum membrane distillation," *J. Memb. Sci.*, vol. 80, no. 1, pp. 21–33, 1993, doi: 10.1016/0376-7388(93)85129-K.
[43] F. Laganà, G. Barbieri, and E. Drioli, "Direct contact membrane distillation: Modelling and concentration experiments," *J. Memb. Sci.*, vol. 166, no. 1, pp. 1–11, 2000, doi: 10.1016/S0376-7388(99)00234-3.
[44] M. Khayet, J. I. Mengual, and T. Matsuura, "Porous hydrophobic/hydrophilic composite membranes: Application in desalination using direct contact membrane distillation," *J. Memb. Sci.*, vol. 252, no. 1–2, pp. 101–113, 2005, doi: 10.1016/j.memsci.2004.11.022.
[45] K. Smolders and A. C. M. Franken, "Terminology for Membrane Distillation," *Desalination*, vol. 72, no. 3, pp. 249–262, Dec. 1989, doi: 10.1016/0011-9164(89)80010-4.
[46] R. W. Schofield, A. G. Fane, and C. J. D. Fell, "Heat and mass transfer in membrane distillation," *J. Memb. Sci.*, vol. 33, no. 3, pp. 299–313, 1987, doi: 10.1016/S0376-7388(00)80287-2.
[47] J. I. Mengual, M. Khayet, and M. P. Godino, "Heat and mass transfer in vacuum membrane distillation," *Int. J. Heat Mass Transf.*, vol. 47, no. 4, pp. 865–875, 2004, doi: 10.1016/j.ijheatmasstransfer.2002.09.001.
[48] L. Eykens, K. De Sitter, C. Dotremont, L. Pinoy, and B. Van Der Bruggen, "How to Optimize the

Membrane Properties for Membrane Distillation: A Review," *Ind. Eng. Chem. Res.*, vol. 55, no. 35, pp. 9333–9343, 2016, doi: 10.1021/acs.iecr.6b02226.
[49] N. Hengl *et al.*, "Study of a new membrane evaporator with a hydrophobic metallic membrane," *J. Memb. Sci.*, vol. 289, no. 1–2, pp. 169–177, 2007, doi: 10.1016/j.memsci.2006.11.051.
[50] M. Khayet, T. Matsuura, J. I. Mengual, and M. Qtaishat, "Design of novel direct contact membrane distillation membranes," *Desalination*, vol. 192, no. 1–3, pp. 105–111, 2006, doi: 10.1016/j.desal.2005.06.047.
[51] J. Phattaranawik, R. Jiraratananon, and A. G. Fane, "Heat transport and membrane distillation coefficients in direct contact membrane distillation," *J. Memb. Sci.*, vol. 212, no. 1–2, pp. 177–193, 2003, doi: 10.1016/S0376-7388(02)00498-2.
[52] M. Rezaei, D. M. Warsinger, J. H. Lienhard V, M. C. Duke, T. Matsuura, and W. M. Samhaber, "Wetting phenomena in membrane distillation: Mechanisms, reversal, and prevention," *Water Res.*, vol. 139, no. 08, pp. 329–352, Aug. 2018, doi: 10.1016/j.watres.2018.03.058.
[53] M. Gryta, "Influence of polypropylene membrane surface porosity on the performance of membrane distillation process," *J. Memb. Sci.*, vol. 287, no. 1, pp. 67–78, 2007, doi: 10.1016/j.memsci.2006.10.011.
[54] M. Gryta, M. Tomaszewska, and A. W. Morawski, "Membrane distillation with laminar flow," *Sep. Purif. Technol.*, vol. 11, no. 2, pp. 93–101, 1997, doi: 10.1016/S1383-5866(97)00002-6.
[55] J. Gilron, Y. Ladizansky, and E. Korin, "Silica fouling in direct contact membrane distillation," *Ind. Eng. Chem. Res.*, vol. 52, no. 31, pp. 10521–10529, 2013, doi: 10.1021/ie400265b.
[56] W. R. Purcell, "Interpretation of Capillary Pressure Data," *J. Pet. Technol.*, vol. 2, no. 08, pp. 11–12, Aug. 1950, doi: 10.2118/950369-G.
[57] M. R. Bilad, E. Guillen-Burrieza, M. O. Mavukkandy, F. A. Al Marzooqi, and H. A. Arafat, "Shrinkage, defect and membrane distillation performance of composite PVDF membranes," *Desalination*, vol. 376, pp. 62–72, 2015, doi: https://doi.org/10.1016/j.desal.2015.08.015.
[58] B. Scientific AB, "Theta Lite," 2018. https://www.biolinscientific.com/attension/optical-tensiometers/theta-lite?utm_term=&utm_campaign=BR-DSA-Attension-G-EN&utm_source=adwords&utm_medium=ppc&hsa_acc=1094516957&hsa_cam=1333847646&hsa_grp=57466913194&hsa_ad=400408274048&hsa_src=g&hsa_tgt=dsa-4 (accessed May 22, 2021).
[59] T. Misono, "Measurement Techniques and Practices of Colloid and Interface Phenomena," *Meas. Tech. Pract. Colloid Interface Phenom.*, pp. 39–44, 2019, doi: 10.1007/978-981-13-5931-6.
[60] dataphysics, "OCA product series," 2018.
[61] S. Ebnesajjad, "3 - Surface Tension and Its Measurement," in *Handbook of Adhesives and Surface Preparation*, S. Ebnesajjad, Ed. Oxford: William Andrew Publishing, 2011, pp. 21–30.
[62] A. B. D. Cassie, "Contact angles," *Discuss. Faraday Soc.*, vol. 3, no. 9, p. 11, 1948, doi: 10.1039/df9480300011.
[63] D. Myers, *Surfactant Science and Technology*. Wiley, 2020.
[64] G. Vazquez, E. Alvarez, and J. M. Navaza, "Surface Tension of Alcohol + Water from 20 to 50 °C," *J. Chem. Eng. Data*, vol. 40, no. 3, pp. 611–614, 1995, doi: 10.1021/je00019a016.
[65] K. S. Howard and R. A. McAllister, "The viscosity of acetone-water solutions up to their normal boiling points," *AIChE J.*, vol. 4, no. 3, pp. 362–366, 1958, doi: 10.1002/aic.690040326.
[66] B. J. Ryan and K. M. Poduska, "Roughness effects on contact angle measurements," *Am. J. Phys.*, vol. 76, no. 11, pp. 1074–1077, 2008, doi: 10.1119/1.2952446.
[67] C. Reichardt and T. Welton, *Solvents and Solvent Effects in Organic Chemistry*. Weinheim, Germany: Wiley-VCH Verlag GmbH & Co. KGaA, 2010.
[68] Y. Marcus, "The use of chemical probes for the characterization of solvent mixtures. Part 2. Aqueous mixtures," *J. Chem. Soc. Perkin Trans. 2*, no. 8, p. 1751, 1994, doi: 10.1039/p29940001751.

Appendix A

Table 16: Curve fittings executed for the LEP equation formulation

Mixture	Parameter	Equation
Methanol-water	Surface tension	$ST(x) = 31.32 * \exp(-10.45 * x) + 39.98 * \exp(-0.5899 * x)$
	Contact angle	$CA(x) = 16.36 * \exp(-6.164 * x) + 94.61 * \exp(-0.4279 * x)$
	Kamlet-Taft	$KT(x) = 0.4371 * x^4 + 0.07576 * x^3 - 0.9636 * x^2 + 0.03642 * x + 1.096$
Ethanol-water	Surface tension	$ST(x) = 42.25 * \exp(-16.36 * x) + 29.06 * \exp(-0.2945 * x)$
	Contact angle	$CA(x) = 34.05 * \exp(-5.535 * x) + 78.07 * \exp(-0.8338 * x)$
	Kamlet-Taft	$KT(x) = -5.682 * x^4 + 12.52 * x^3 - 8.71 * x^2 + 1.317 * x + 1.097$
Acetic acid-water	Surface tension	$ST(x) = 29.6 * \exp(-17.34 * x) + 41.7 * \exp(-0.4725 * x)$
	Contact angle	$CA(x) = 12.65 * \exp(-400.4 * x) + 97.55 * \exp(-0.5313 * x)$
	Kamlet-Taft	$KT(x) = -3.409 * x^4 + 7.166 * x^3 - 5.071 * x^2 + 0.8018 * x + 1.091$
Acetone-water	Surface tension	$ST(x) = 38.54 * \exp(-19.68 * x) + 32.77 * \exp(-0.3672 * x)$
	Contact angle	$CA(x) = 27.42 * \exp(-381.9 * x) + 82.78 * \exp(-0.6973 * x)$
	Kamlet-Taft	$KT(x) = -1.399 * x^4 + 3.023 * x^3 - 1.84 * x^2 - 0.1847 * x + 1.091$
Acetonitrile-water	Surface tension	$ST(x) = 39.48 * \exp(-13.74 * x) + 31.83 * \exp(-0.03602 * x)$
	Contact angle	$CA(x) = 34.22 * \exp(-19.98 * x) + 76.04 * \exp(-0.2128 * x)$
	Kamlet-Taft	$KT(x) = -4.108 * x^4 + 8.013 * x^3 - 4.454 * x^2 + 0.1988 * x + 1.098$

x: concentration of the organic component, expressed in mol percent (as a decimal)

Table 17: R-square and adjusted R-square for the fitting equations

Equation	R-square	Adjusted R-square
$ST(x) = 31.32 * \exp(-10.45 * x) + 39.98 * \exp(-0.5899 * x)$	0.9997	0.9988
$CA(x) = 16.36 * \exp(-6.164 * x) + 94.61 * \exp(-0.4279 * x)$	0.9915	0.9787
$KT(x) = 0.4371 * x^4 + 0.07576 * x^3 - 0.9636 * x^2 + 0.03642 * x + 1.096$	0.9964	0.9939
$ST(x) = 42.25 * \exp(-16.36 * x) + 29.06 * \exp(-0.2945 * x)$	1	0.9999
$CA(x) = 34.05 * \exp(-5.535 * x) + 78.07 * \exp(-0.8338 * x)$	0.9828	0.957
$KT(x) = -5.682 * x^4 + 12.52 * x^3 - 8.71 * x^2 + 1.317 * x + 1.097$	0.9986	0.9977
$ST(x) = 29.6 * \exp(-17.34 * x) + 41.7 * \exp(-0.4725 * x)$	0.9999	0.9997
$CA(x) = 12.65 * \exp(-400.4 * x) + 97.55 * \exp(-0.5313 * x)$	0.9252	0.8131
$KT(x) = -3.409 * x^4 + 7.166 * x^3 - 5.071 * x^2 + 0.8018 * x + 1.09$	0.9999	0.9998
$ST(x) = 38.54 * \exp(-19.68 * x) + 32.77 * \exp(-0.3672 * x)$	0.9999	0.9998
$CA(x) = 27.42 * \exp(-381.9 * x) + 82.78 * \exp(-0.6973 * x)$	0.9757	0.9392
$KT(x) = -1.399 * x^4 + 3.023 * x^3 - 1.84 * x^2 - 0.1847 * x + 1.091$	0.9999	0.9998
$ST(x) = 39.48 * \exp(-13.74 * x) + 31.83 * \exp(-0.03602 * x)$	1	1
$CA(x) = 34.22 * \exp(-19.98 * x) + 76.04 * \exp(-0.2128 * x)$	0.9992	0.9979
$KT(x) = -4.108 * x^4 + 8.013 * x^3 - 4.454 * x^2 + 0.1988 * x + 1.098$	0.995	0.9916

x: concentration of the organic component, expressed in mol percent (as a decimal)